Directly Deposited Silicon/Graphene Hybrid Anodes for Li-ion Batteries

A Thesis

Presented to the Faculty of the Graduate School

of Cornell University

In Partial Fulfillment of the Requirements for the Degree of

Master of Science

by

Leyan Wang

August, 2019

ABSTRACT

Lithium-ion batteries (LIB) are considered as the most essential energy storage systems due to high energy density. However, current graphite anodes severely hinder LIB from further supporting fast-growing electric vehicles markets for low theoretical capacity. Silicon attracts attentions as one of the most promising candidates for next-generation LIB anode materials because of its much higher theoretical capacity. Silicon anodes have not been commercialized because of the challenges caused by extreme volume expansions and following passive problems, including continuous solid electrolyte interface formation, contact loss between active materials and finally, cycle retention decays. In this thesis, we discuss how to overcome these technical issues by engineering Si/graphene hybrid anodes through air-controlled electrospray, which include three parts: silicon/graphene hybrid additive to LIB anode with Modifications; directly deposited silicon/graphene oxide LIB anode and further study on their size ratio effect and finally Interconductivity from graphene nanoribbon (GNR) in directly deposited silicon/graphene LIB anode.

BIOGRAPHICAL SKETCH

Leyan Wang was born in China, on November 13, 1995. Her interest in science and technology aroused since young age. She was admitted by University of Washington after graduating from high school and decided to choose Chemical Engineering as major after one-year undergraduate study. She then moved to east coast and joined Master of Science at Cornell University, Robert Frederick Smith School of Chemical and Biomolecular Engineering. At Cornell University, she performed scientific research in developing next generation Lithium-ion batteries.

ACKNOWLEDGMENTS

I would like to thank my advisor and best teacher Professor Yong L. Joo for including me in his research group and his guidance and advices through my two-year MS study. I would also like to thank my committee member Professor Tobias Hanrath for his valuable inputs and suggestions.

I would like to extend my special thanks to Park Sang Mok and Dr Jin Hong Lee for your patient helps and trainings that are useful in energy storage field research and the rest of the Joo group members for your generous suggestions.

Finally, I would like to express my gratitude to my parents for their love and support for every of my decisions and provide me with chance to study at Cornell University.

Table of Contents

CHAPTER 1

Introduction

1.1 Lithium-ion Battery Overview

Currently, a revolution that transferring vehicles from relying on internal combustion engines to electric vehicles is going on positively. Lithium-ion batteries stand out and become market leader because of its high energy density, exceptional rate capabilities, lasting cycle life and improved safety level with wide operation temperature window and some researchers have claimed that Li-ion batteries can be considered as one of the most essential inventions in electrochemistry during the last two decades [1,2]. Composed mainly of positive electrode (cathode), negative electrode (anode), electrolyte and separator, Li-ion batteries are also known as rocking-chair batteries because of their two-way lithium ion movement. Lithium ions extract from cathode, migrate through ion-conductive electrolyte, then intercalate on anode during charging process and conversely, migrate back to cathode during discharge. During the process, chemical reactions occur at electrode-electrolyte interface and electric energy is collected. [3-5].

Yet, fast-growing electric automobile industry raises up requirements for energy storage devices and current Li-ion batteries is in fact, lagging far from these new demands, such as higher capacity and fast charge/discharge. To overcome this gap, many studies have been performed to improve different battery components from either electrochemical performances or safety perspective. Various carbon materials, such as graphene/graphene oxide [6-9] were incorporated with cathode system to build 3D conductive network for better Li^+ infusion and enhance both capacity and capability. Composite cathodes which integrate two electrode materials also show improved electrochemical performances due to extra protective layer [10-12]. Separators coated with thin ceramic layer, composed of Al_2O_3 nano powder and various kinds of binders [13-15], attract researchers' attention because of proved improvements in thermal stability at high temperature and this technology has been applied in electric vehicle industry.

Furthermore, researches on gel electrolyte, which is committed to overcoming security issues from traditional organic liquid electrolyte, has been confirmed as a good substitute of traditional liquid electrolyte [16,17].

We can see technical progresses in all parts of Li-ion batteries, which have been put into commercialization, except anode materials. Lithium-ion batteries' anode has been made with graphite since it was introduced in 1991 until current time [18]. Graphite, in fact, is a suitable holder due to the small potential difference in between lithium and lithium graphite intercalation, which makes graphite able to keep structure integrity [4]. Moreover, graphite's layered structure prevents lithium dendrites formation, which is a huge risk of short-circuit [19]. However, graphite has relatively low theoretical capacity (372 mAh/g) and has also been reached almost 30 year ago [18]. Therefore, a breakthrough in lithium-ion battery anode is in urgent need. Silicon is considered as one of the most promising anode materials for lithium-ion batteries due to its natural abundance, low working potential and high theoretical gravimetric capacity (4200 mAh/g) [19,20]. However, many problems hinder Si application into Lithium-ion battery. First, there are up to 400% volume expansion and contraction during lithiation/de-lithiation process, which will further lead to electrical disconnection between active materials, instable solid electrolyte interface (SEI) and severe capacity decay [21,22]. Second, silicon has intrinsic low ionic/electrical conductivity [22] which make silicon utilization relies heavily on conductive materials.

Many attempts have been made in order to concur these technical issues and one of the most popular approaches is to build Si/Carbon matrix anode system. The most commonly used carbon material is graphene, which is a monolayer of carbon atoms arranged as honeycomb crystal lattice and has features of superior electrical conductivity, remarkable chemical stability and mechanical strength and high surface area around 2600 $m^2 g^{-1}$ [23,24]. Another common carbon material is graphene oxide, which is graphene bearing oxygen functional groups [25]. Moreover, by silicon itself, downsizing into nanoscale

or microscale particles can significantly improve silicon stabilization and cycle life. Nanostructured silicon with different morphologies, such as Si nanowire [26-28] and Si nanotube [29] have been proved to accommodate strain, reduce Si pulverization effectively and accommodate severe Si anode cycle life decay. In Si/Carbon composite system, carbon mostly acts as electrode conductive pathways to enhance silicon utilization and supports the system integrity [30]. Advanced nanostructured electrode systems, including Si/C core-shell nanowire anode [30], carbon nanotube (CNT)-silicon hybrid anode [31,32] and graphite encapsulated silicon nanowire anode [33], all showed much higher specific capacity comparing with that of traditional graphite anode and improved cycling performance.

In our study, we are focusing on combining merits of carbon materials and silicon nanoparticles/micro-particles through producing Si/C hybrids systems through air-controlled electrospray method. The novel deposition method allows us to get target electrode morphology by simply adjusting parameters such as voltage and air pressure when conducting. This prominent advantage makes air-controlled electrospray adaptable for all works that will discussed in this thesis work. As results, silicon can be utilized efficiently with sufficient conductive pathways while its volume expansion either trapped by carbon materials or relaxed due to deliberately created inner void spaces. More details about air-controlled electrospray is introduced in the following section.

1.2 Air-controlled Electrospray

Electrospraying is a robust technique that takes use of electrical force, usually high voltage up to order of several kilovolts to reduce liquid droplet size down to nanometer from bulk solution with controls in products' composition, morphology and shape and has been broadly applied in nanoscale fabrications since 1990s [34-36]. Air-controlled electrospray is a coaxial system with inner needle constrains solution and outer shell build channels for air to distribute evenly, which inherits all merits of electrospray, such as decrease in droplet size and no extra drying step [37]. Moreover, air helps further atomize solutions,

accelerate solvent evaporation and spray process several times faster than electrospray and uniform deposit droplets onto collector [38].

References

[1] V. Etacheri, R. Marom, R. Elazari, G. Salitra, D. Aurbach, Challenges in the development of advanced Li-ion batteries: A review. Energy & Environmental Science. 4 (2011) 3243–3262. doi:10.1039/c1ee01598b.

[2] L. Ji, Z. Lin, M. Alcoutlabi, X. Zhang, Recent developments in nanostructured anode materials for rechargeable lithium-ion batteries. Energy & Environmental Science. 4 (2011) 2682–2699. doi:10.1039/c0ee00699h.

[3] C. Daniel, Materials and processing for lithium-ion batteries. The Journal of The Minerals, Metals & Materials Society. 60 (2008).

[4] M. Wakihara, Recent developments in lithium ion batteries. Materials Science and Engineering: R: Reports. 33 (2001) 109-134. doi:10.1016/S0927-796X(01)00030-4.

[5] J. Tarascon, M. Armand, Issues and challenges facing rechargeable lithium batteries. Nature. 414 (2001) 359-367. doi:10.1038/35104644.

[6] X. Zhou, F. Wang, Y. Zhu, Z. Liu, Graphene modified LiFePO4 cathode materials for high power lithium ion batteries. Journal of Materials Chemistry. 21 (2011) 3353-3358. doi:10.1039/c0jm03287e.

[7] L. Hu, F. Wu, C. Lin, A.N. Khlobystov, L. Li, Graphene-modified LiFePO4 cathode for lithium ion battery beyond theoretical capacity. Nature Communications. 4 (2013). doi:10.1038/ncomms2705

[8] J. Yang, J. Wang, D. Wang, X. Li, D. Geng, G. Liang, M. Gauthier, R. Li, X. Sun, 3D porous LiFePO4/graphene hybrid cathodes with enhanced performance for Li-ion batteries. Journal of Power Sources. 208 (2012) 340-344. doi: 10.1016/j.jpowsour.2012.02.032.

[9] Y. Shi, S. Chou, J. Wang, D. Wexler, H. Li, H. Liu, Y. Wu, Graphene wrapped LiFePO4/C composites as cathode materials for Li-ion batteries with enhanced rate capability. Journal of Materials Chemistry. 22 (2012) 16465-16470. doi:10.1039/c2jm32649c.

[10] G. Li, Z. Yang, W. Yang, Effect of FePO4 coating on electrochemical and safety performance of LiCoO2 as cathode material for Li-ion batteries. Journal of Power Sources. 183 (2008) 741-748. doi:10.1016/j.jpowsour.2008.05.047.

[11] J.H. Shim, N.H. Cho, S. Lee, Synthesis and characterization of Mg2TiO4-coated LiCoO2 as a cathode material for lithium ion batteries. Electrochimica Acta. 243 (2017) 162-169. doi:10.1016/j.electacta.2017.05.073.

[12] N. Taguchi, T. Akita, K, Tatsumi, H. Sakaebe, Characterization of MgO-coated-LiCoO2 particles by analytical transmission electron microscopy. Journal of Power Sources. 328 (2016) 161-166. doi:10.1016/j.jpowsour.2016.07.116.

[13] J. Choi, S.H. Kim, D. Kim, Enhancement of thermal stability and cycling performance in lithium-ion cells through the use of ceramic-coated separators. Journal of Power Sources. 195 (2010) 6192-6196. doi:10.1016/j.jpowsour.2009.11.020.

[14] H. Jeong, D. Kim, Y.U. Jeong, S. Lee, Effect of phase inversion on microporous structure development of Al2O3/poly(vinylidene fluoride-hexafluoropropylene)-based ceramic composite separators for lithium-ion batteries. Journal of Power Sources. 195 (2010) 6116-6121. doi:10.1016/j.jpowsour.2009.10.085.

[15] C. Shi, P. Zhang, L. Chen, P. Yang, P., J. Zhao, J, Effect of a thin ceramic-coating layer on thermal and electrochemical properties of polyethylene separator for lithium-ion batteries. Journal of Power Sources, 270 (2014) 547-553. doi:10.1016/j.jpowsour.2014.07.142.

[16] A.M. Stephan, Review on gel polymer electrolytes for lithium batteries. European Polymer Journal, 42 (2006) 21-42. doi:10.1016/j.eurpolymj.2005.09.017.

[17] J.Y. Song, Y.Y. Wang, C.C. Wan, Review of gel-type polymer electrolytes for lithium-ion batteries. Journal of Power Source, 77 (1999) 183-197. doi:10.1016/S0378-7753(98)00193-1.

[18] N.Y. Kim, C. Oh, J.Y. Kim, J.S. Kim, E.D. Jeong, J.S. Bae, J.K. Lee, High-Performance Li-Ion Battery Anodes Based on Silicon-Graphene Self-Assemblies. Journal of The Electrochemical Society. 164 (2017) A6075-A6083. doi: 10.1149/2.0101701jes.

[19] A. Casimir, H. Zhang, O. Ogoke, J.C. Amine, J. Lu, G. Wu, Silicon-based anodes for lithium-ion batteries: Effectiveness of materials synthesis and electrode preparation. Nano Energy, 27 (2016) 359-376. doi:10.1016/j.nanoen.2016.07.023.

[20] X. Zuo, P. Müller-Buschbaumb, Y-J. Cheng, Silicon based lithium-ion battery anodes: A chronicle perspective review. Nano Energy, 31 (2017) 113-143. doi:10.1016/j.nanoen.2016.11.013.

[21] V. Chabot, K. Feng, H.W. Park, F.M. Hassan, A.R. Elsayed, A. Yu, X. Xiao, Z. Chen, Graphene wrapped silicon nanocomposites for enhanced electrochemical performance in lithium ion batteries. Electrochimica Acta, 130 (2014) 127-134. doi:10.1016/j.electacta.2014.02.135.

[22] C. Fu, G. Zhao, H. Zhang, S. Li, Evaluation and Characterization of Reduced Graphene Oxide Nanosheets as Anode Materials for Lithium-Ion Batteries. Int. J. Electrochem. Sci.. 8 (2013) 6269 – 6280.

[23] L. Ji, H. Zheng, A. Ismach, Z. Tan, S. Xun, E. Lin, E., V. Battagalia, V. Srinizasan, Y. Zhang, Graphene/Si multilayer structure anodes for advanced half and full lithium-ion cells. Nano Energy. 1 (2012) 164-171. doi:10.1016/j.nanoen.2011.08.003.

[24] E. Yoo, J. Kim, E. Hosono, H. Zhou, T. Kudo, I. Honma, Large Reversible Li Storage of Graphene Nanosheet Families for Use in Rechargeable Lithium Ion Batteries. Nano Letters. 8 (2008) 2277-2282. doi:10.1021/nl800957b.

[25] D.A. Dikin, S. Stankovich, E.J. Zimney, R.D. Piner, G.H.B. Dommett, G. Evmenenko, S.Y. Nguyen, R.S. Ruoff, Preparation and characterization of graphene oxide paper. Nature. 448 (2007) 457-460. doi:10.1038/nature06016.

[26] A.M. Chockla, J.T. Harris, V.A. Akhavan, T.D. Bogart, V.C. Holmberg, C. Steinhagen, C.B. Mullins, K.J. Stevenson, B.A. Korgel, Silicon Nanowire Fabric as a Lithium Ion Battery Electrode Material. Journal of the American Chemical Society. 133 (2001) 20914-20921. doi:10.1021/ja208232h.

[27] C.K. Chan, H. Peng, G. Liu, K. Mcilwrath, X.F. Zhang, R.A. Huggins, Y. Cui, High-performance lithium battery anodes using silicon nanowires. Nature Nanotechnology. 3 (2007) 31-35. doi:10.1038/nnano.2007.411.

[28] M. Ge, J. Rong, X. Fang, C. Zhou, C, Porous Doped Silicon Nanowires for Lithium Ion Battery Anode with Long Cycle Life. Nano Letters. 12 (2012) 2318-2323. doi:10.1021/nl300206e.

[29] M.H. Park, M.G. Kim, J. Joo, K. Kim, J, Kim, S. Ahn, Y. Cui, J. Cho, Silicon nanotube battery anodes. Nano Letter. 9 (2009) 3844-3847. doi:10.1021/nl902058c.

[30] L. Cui, Y. Yang, C. Hsu, Y. Cui, Carbon–Silicon Core–Shell Nanowires as High Capacity Electrode for Lithium Ion Batteries. Nano Letters. 9 (2009) 3370-3374. doi:10.1021/nl901670t.

[31] L. Cui, L. Hu, J.W. Choi, Y. Cui, Light-Weight Free-Standing Carbon Nanotube-Silicon Films for Anodes of Lithium Ion Batteries. ACS Nano. 4 (2010) 3671-3678. doi:10.1021/nn100619m.

[32] W. Wang, P.N. Kumta, Nanostructured Hybrid Silicon/Carbon Nanotube Heterostructures: Reversible High-Capacity Lithium-Ion Anodes. ACS Nano. 4 (2010) 2233-2241. doi: 10.1021/nn901632g.

[33] B. Wang, X. Li, X. Zhang, B. Luo, Y. Zhang, L. Zhi, Contact-Engineered and Void-Involved Silicon/Carbon Nanohybrids as Lithium-Ion-Battery Anodes. Advanced Materials. 25 (2013) 3560-3565. doi:10.1002/adma.201300844.

[34] A. Jaworek, A.T. Sobczyk, Electrospraying route to nanotechnology: An overview, J. Electrostat. 66 (2008) 197–219. doi:10.1016/j.elstat.2007.10.001.

[35] J. Xie, P. Jiang, M. Davoodi, M. Srinivasan, C. Wang, Electrohydrodynamic atomization: A two-decade effort to produce and process micro-/nanoparticulate materials. Chemical Engineering Science. 125 (2015) 32-57. doi: 10.1016/j.ces.2014.08.061.

[36] S. K. Boda, X. Li, J. Xie, Electrospraying an enabling technology for pharmaceuticaland biomedical applications: A review. Journal of Aerosol Science. 125 (2018) 164-181. doi: 10.1016/j.jaerosci.2018.04.002.

[37] J. Lee, B. Ko, J. Kang, Y. Chung, Y. Kim, W. Halim, J.H. Lee, Y.L. Joo, Facile and scalable fabrication of highly loaded sulfur cathodes and lithium–sulfur pouch cells via air-controlled electrospray, Mater. Today Energy. 6 (2017) 255–263. doi:10.1016/j.mtener.2017.11.003.

[38] L. Fei, S.H. Yoo, R.A.R. Villamayor, B.P. Williams, S.Y. Gong, S. Park, K. Shin, Y.L. Joo, Graphene Oxide Involved Air-Controlled Electrospray for Uniform, Fast, Instantly Dry, and Binder-Free Electrode Fabrication, ACS Appl. Mater. Interfaces. 9 (2017) 9738–9746. doi:10.1021/acsami.7b00087.

Chapter 2

Silicon/Graphene Hybrid Additive to Li-ion Batteries Anode with Modifications

2.1 Introduction

Stepping into neutral-carbon era, electric vehicles (EVs) and plug-in hybrid electric vehicles (PHEVs) substituting traditional fuel-consuming vehicles becomes an irreversible trend. Thus, energy storage source which is portable, of high capacity and long cycle life is in large demand and lithium ion batteries (LIB) play an important role as rechargeable batteries which potentially own these properties [1]. However, current lithium ion batteries (LIB) are not ideal enough to support increasing requirements and we need to further enhance LIB energy content and structure design [1]. Many efforts have been put in to improve cathode capacities by either designing better electrode architecture, such as modifying lithium iron phosphate with thin layer graphene [2], synthesizing $LiFePo_4$ as open three-dimensional porous structure [3], or choosing Li-rich cathode materials such as Li-rich layered $Li(Li_{0.17}Ni_{0.25}Mn_{0.58})O_2$ [4]. Despite progresses in LIB cathode research, LIB anodes are still made of graphite. Even though graphite's layered structure makes it a suitable holder for lithium ion, its theoretical capacity (372 mAh/g) is very limited and has been achieved since 1991 [5].

Silicon (Si) has been considered as the most promising candidate as newly LIB anode materials because of its more than 10 times higher theoretical capacity (4200 mAh/g) at full lithiation ($Li_{22}Si_5$) comparing with that of graphite [6]. Moreover, Si's low working potential ($0 - 0.4V$ vs. Li/Li^+), low cost and natural abundance set it to be replacement of graphite [7]. Unfortunately, there are several drawbacks that hinder Si-only lithium-ion battery anode applications. First, Si goes through up to 320% volume expansion during lithiation and shrinks back to vary volumes during de-lithiation due to large amount of Li-ion intercalation/de-intercalation, which will potentially cause cracks on electrode and disconnections between active materials with surrounding during cycling [8]. The other issue comes from continuous formation of solid-electrolyte interface (SEI), which is formed due to decomposition of organic electrolyte

on electrode surface and is ionically conductive and electronically insulating [9]. A densely packed, firmly adhesive and flexible SEI can be very helpful as electrode protection layer. It is useful in holding system integrity, preventing loss of lithium ions results from silicon's continuous pulverization and stopping corrosion of anode [10]. However, continuous cracks expose fresh electrode's surface which will contact with electrolyte and trigger continuous SEI formation. These side reactions lead to lower Coulombic efficiency, severe electrode degradation, cell capacity decay and lack of electrode conductive pathways between Si and current collector [9-12]. Taking use of nano-structured silicon, such as Si nanowire, Si nanotube and porous nano Si nanoparticle [9, 12-17], slightly alleviates previous problems, but improvement is not good enough for commercialization. To control SEI formation, more advanced Si/C hybrid electrodes were introduced and have been engineered in several different ways, including Si nanoparticles dispersion in between graphene sheets [15] and graphene-encapsulated Si nanoparticles [18]. These Si/C hybrid systems yielded higher Coulombic efficiency and more stable cycle retention comparing with bare Si nanoparticles. However, more challenges come from intrinsic disadvantages of nanostructured silicon electrodes [14], such as low inner conductivity and large inter-particle resistance. Thus, more modifications are required for Si nanoparticles included electrode in order to utilize nanostructured Silicon effectively.

As mentioned before, as key role in Si-C electrode network, graphene becomes a research hot spot in recent year because of its 2D extendable honeycomb network, strong mechanical strength, chemically stability and high specific surface area (SSA is 2630 m^2g^{-1}) comparing with 3D graphite [19, 20] and these properties solidify graphene's feasibility as inner conductive channels for lithium-ion battery electrode [21]. Graphene is not ideal lithium-ion battery anode material if it is used for capacity storage. In order to take advantages of graphene's superior 2D structure properties and mitigate challenges stated previously, we take use of graphene as both conductive pathways that connect Si nanoparticles inside Si nanoparticle

(SiNP)/Graphene nano composites and protection layer in between electrode and electrolyte, thus solving lithium-ion battery's severe lifetime decay.

In this study, we implement air-controlled electrospray method, which was inspired by industrialized electrospinning process [22], to first synthesize SiNP/Graphene nano composites (Si/Gr). Si/Gr is a spherical/ potato-like composite with good graphene inter-connecting, thus SiNPs can be utilized more efficiently comparing with commercial SiNPs. We then add Si/Gr into graphite anode as additives along with excess amount of binder via air-controlled electrospray method again. After binder removal through thermal annealing, electrode inner void spaces which can accommodate silicon volume expansion and relax strains are thus created. We can see improvement in capacity comparing with that of traditional graphite anodes. Considering intrinsic drawbacks from nanostructured electrode stated before and further controlling SEI formation, we modify system with calendaring, adding extra graphene layer via air-controlled electrospray or combination of both approaches. Modified systems' specific capacity, Coulombic efficiency and cycle retention for long cycles at 1.26 Ahg^{-1} are compared with those of unmodified system. Materials synthesis and coating are mostly conducted through air-controlled electrospray method, which is a simple and non-toxic process [22].

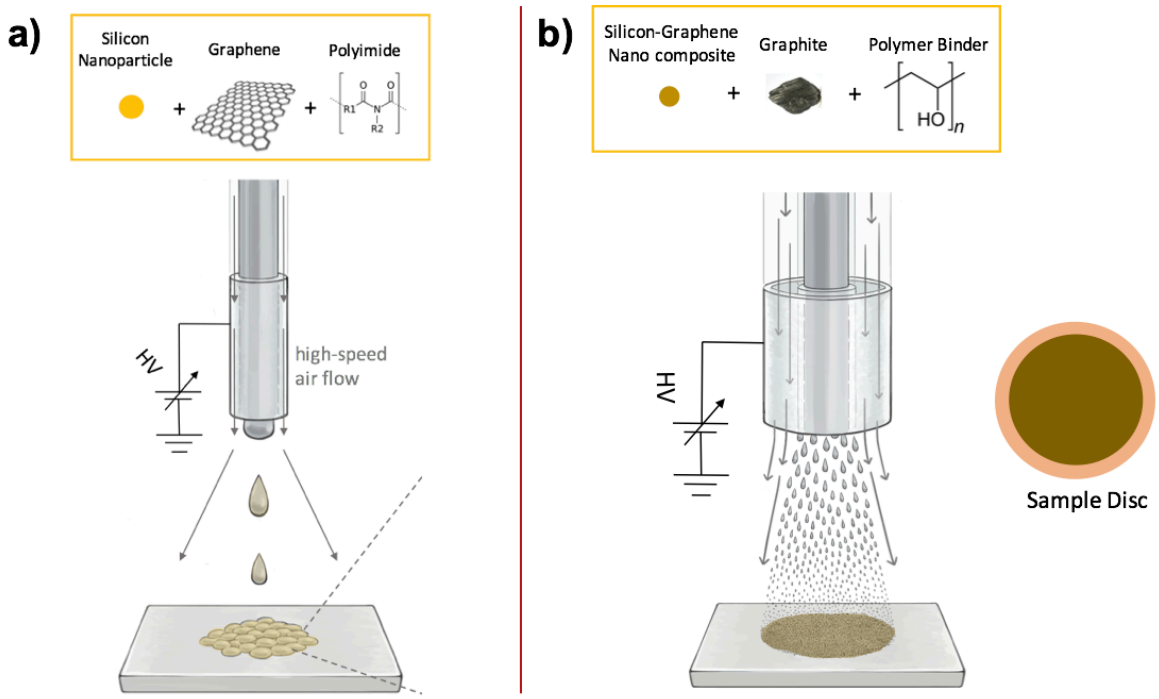

Fig. 2.1. Schematic illustrations of **a)** air-controlled electrospray process for Si/Gr nano composite formation. **b)** air-controlled electrospray process for electrode preparation and sample disc.

2.2 Experimental Section

2.2.1 Preparation of Si/Gr Slurry

Si/Gr nano composites were prepared by turning solution slurry into coating on aluminum current collector via air-controlled electrospray method. Si/Gr could be easily rubbed off from aluminum substrate and was further grinded by laboratory Mortar grinding tool. **Figure. 2.1a** shows main manufacture process of Si/Gr nano composites. The slurry was composed of SiNPs (US Research Nanomaterials Inc., 98+%, 30-50nm), graphene aqueous suspension (ACS Materials, 5wt% graphene sheets, 95 wt% NMP), and polyimide with NMP and DMF as co-solvent (1:1) in the solid weight ratio of 6: 2: 2. 3.5g graphene solution with additional 1.9g NMP and 5.2g DMF were mixed and vortexed 5 min until homogenous. 0.5g SiNPs was then added into previous solution and sonicated (Qsonic) for at least 1 h following by adding 6.7g

PI binder solution. Solution was stirred overnight before spraying and overall solid content is around 6.5 wt%. The air-controlled electrospray takes use of Harvard Apparatus PHD 2000 infusion syringe pump, with working voltage of 25 kV and air pressure of 25 psi. Distance (from needle tip to collector) is around 20 cm and solution was pumped out of inner needle at infusion rate of 0.01 mL/min. After finishing electrospray, collector was removed from instruments and particles were gently rubbed off from collector surface. After being grained twice, dark-greenish fine powder was achieved for further use.

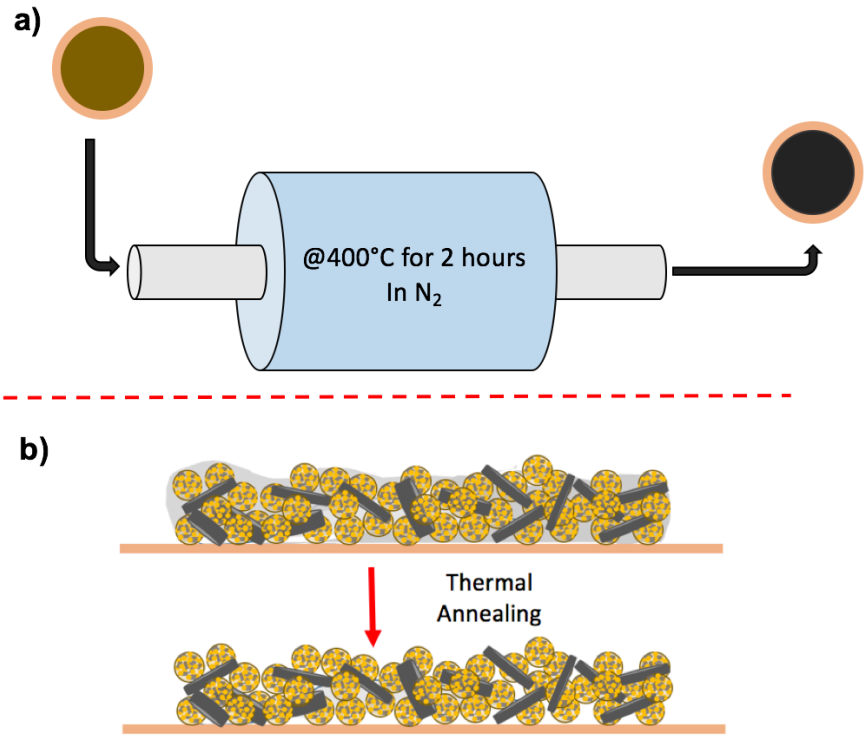

Fig. 2.2. Schematic illustration of **a)** process of disc thermal annealing **b)** disc cross-section before and after thermal annealing.

2.2.2 Preparation of LI-ion Battery Anode

Air-controlled electrospray method was further used for Li-ion battery anode preparation with same instrument. CP11 graphite was diluted with deionized (DI) water into 5 wt% solution and

ultrasonicated (Qsonic) 2h for better dispersion. 3.1g poly(vinyl alcohol) (PVA) (5 wt%) and 0.034g styrene-butadiene rubber (SBR) (50 wt%) were mixed with weight ratio 9:1 and diluted with 3.6g DI water. After being stirred to homogenous state, solution was added with 0.476g carbon nanotube (CNTs) solution (4.5 wt%) as conductive agent and ultrasonicated (Qsonic) for 10 min. 0.15g prepared Si/Gr and 3.9g CP11 graphite solution were mixed with previous solution accordingly and each step required 5-min vortex until solution reached stable suspension. Air-controlled electrospray was performed under 25kV, 20cm, 0.05 mL/min and 25 psi and it took around 10 min to prepare one disc with target loading 0.4 to 0.5 g/cc (Figure. 2.1b). To remove excess PVA binder and create inner void space that accommodate severe silicon volume expansion, disks were thermally annealed at 350°C in Ar atmosphere (MTI Tube Furnace) at a ramp of 5°C/min for 3 hrs as referred to **Figure. 4.2a**. **Figure. 4.2b** shows schematic illustrations of disc cross-section before and after thermal annealing.

2.2.3 Modification of Prepared Li-ion Battery Anode

After thermal annealing, removal of excess binder would create porous inner structure as well as a rough electrode surface. Concerns about potential risk of losing contact in between active materials came up so that calendaring step was added before heat treatment. After being pressed into thinner disc, electrode density was then increased from 0.5 g/cc to 0.8 g/cc, resulting into a highly packed structure with improved volumetric energy density. Another modification was adding an extra conductive graphene layer on top of disk to protect system's integrity by decreasing SiNPs contact with electrolyte during cycling without hindering SiNPs' contributions to capacity. Moreover, because of its mechanical strength, graphene layer constrained silicon volume expansion from outer.

2.2.4 Physical Characterization

The morphologies of Si/Gr nano composite and Si/Gr/Graphite (Si/Gr/Grpt) anode before and after thermal annealing were characterized by scanning electron microscopy (SEM, LEO 1550 FESEM). The elementary distribution on anode was determined by energy dispersive X-ray (EDS, LEO 1550). Functional group changes before and after thermal annealing were shown by Bruker Vertex V80V Vacuum FTIR system. Electrode composition was determined by thermogravimetric analysis (TA Instrument Q500) from 20°C to 900°C at ramp 10°C/min under air atmosphere.

2.2.5 Electrochemical Characterization

Electrochemical characterizations were conducted on 2032CR coin cells. Si/Gr/Grpt anode was used as half-cell anode and lithium foil as counter electrode. Homemade 1M LiPF6 in fluoroethylene carbonate and dimethyl carbonate (50:50 wt/wt%) electrolyte was selected as electrolyte. Separator in between electrode was polypropylene membrane (Celgard, USA). Cell assembly was performed in an argon-filled glovebox. Galvanostatic charge/ discharge process was tested under 0.01 – 1.5V voltage window versus Li/Li^+ with 3 initial formation cycles at 0.18 Ag^{-1}, and at 1.26 Ag^{-1} for further cycles using battery analyzer (MTI). More electrochemical properties were characterized such as Electrochemical Impedance Spectroscopy (EIS, PARSAT 4000, Princeton applied research), which was performed with amplitude of 10 mV in frequency range 0.1 Hz – 100 kHz. Capacities reported were calculated into specific capacities, which count total weight of disc excluding copper substrate.

2.3 Results and Discussions

2.3.1 Air-controlled electrospray

As mentioned before, air-controlled electrospray method is inspired by electrospinning method [22]. Different from electrospinning, additional air flow helps decreasing particle size and

further forming smoother coating composed of Si/Gr, which is not achievable through traditional slurry coating. Solvent also evaporates before contacting with collector so that no extra drying step is necessary [22]. A co-axial system composed of inner needle with diameter 17G and outer 12G is taken use for this method and composed of inner needle that constrains solution and thus limits particle size effectively and outer needle creates channels to assist air flow more evenly. Besides benefits stated before, air plays another essential rule to accelerate electrospray process [23] and 8 h spray is enough to prepare 0.2 g high-quality Si/Gr nano composites. Moreover, disc preparation process is much faster than traditional coating methods such as drop-casting and slurry coating.

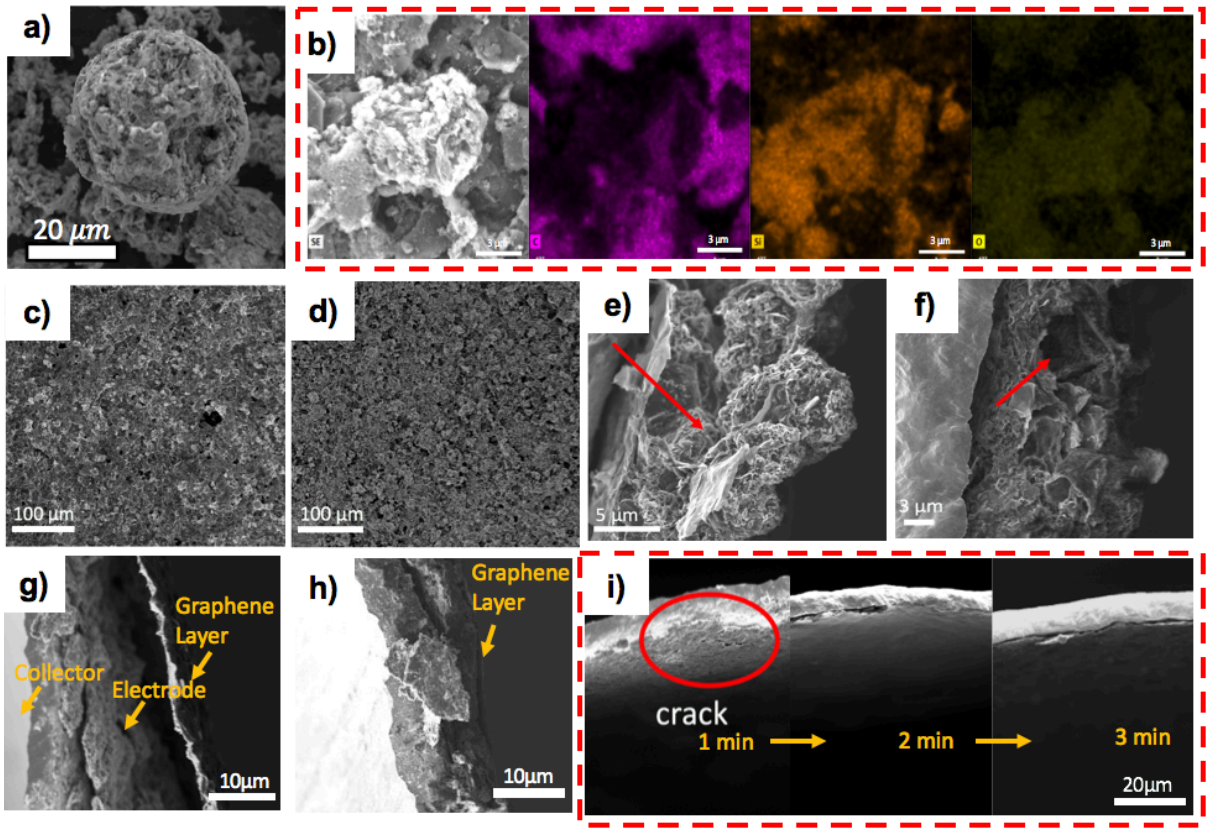

Fig. 2.3. Scanning electron microscopy image of **a)** Si/Gr nano composite. Energy dispersive X-ray image of **b)** Si/Gr nano composite. Scanning electron microscopy images of **c)** Si/Gr/Grpt electrode surface before thermal annealing **d)** Si/Gr/Grpt electrode surface after thermal annealing **e)** cross-section of Si/Gr/Grpt electrode after thermal annealing **f)** cross-

section of thermal annealed Si/Gr/Grpt electrode with compression **g)** cross-section of Si/Gr/Grpt electrode without compression covered by graphene layer **h)** cross-section of Si/Gr/Grpt electrode with compression covered by graphene layer **i)** cross sections of graphene layer with loading 0.04 $mgcm^{-2}$, 0.06 $mgcm^{-2}$, and 0.1 $mgcm^{-2}$.

2.3.2 SiNP-Graphene Nano Composites

Through air-controlled electrospray method, Si/Gr hybrid composites are formed and their spherical structure is shown clearly (Figure. 2.3a). Graphene either wraps or interact in between silicon nanoparticles firmly and the favored spherical morphology give adequate silicon exposure for chemical reactions. SiNP itself has limited lithium diffusion kinetics and low electrical conductivity [24] and this silicon particle and conductive agent hybrid structure facilitates Li ions movements by creating some conductive pathways among active materials. Si/Gr nano composites maintain structural integrity successfully after thermal annealing, thanking for both PI's high-temperature stability and graphene's superior mechanical strength. As we can see from **Figure. 2.3b**, on electrode surface, most SiNPs are still trapped by the Si/Gr firmly. Comparisons between PVA and PI's degradation curves are shown in **Figure. 2.4a**. We take advantages of differences in degradation temperatures of different types of polymers to create inner void space without causing detachment issues and also decide thermal annealing temperature according to this TGA result, which is 350℃.

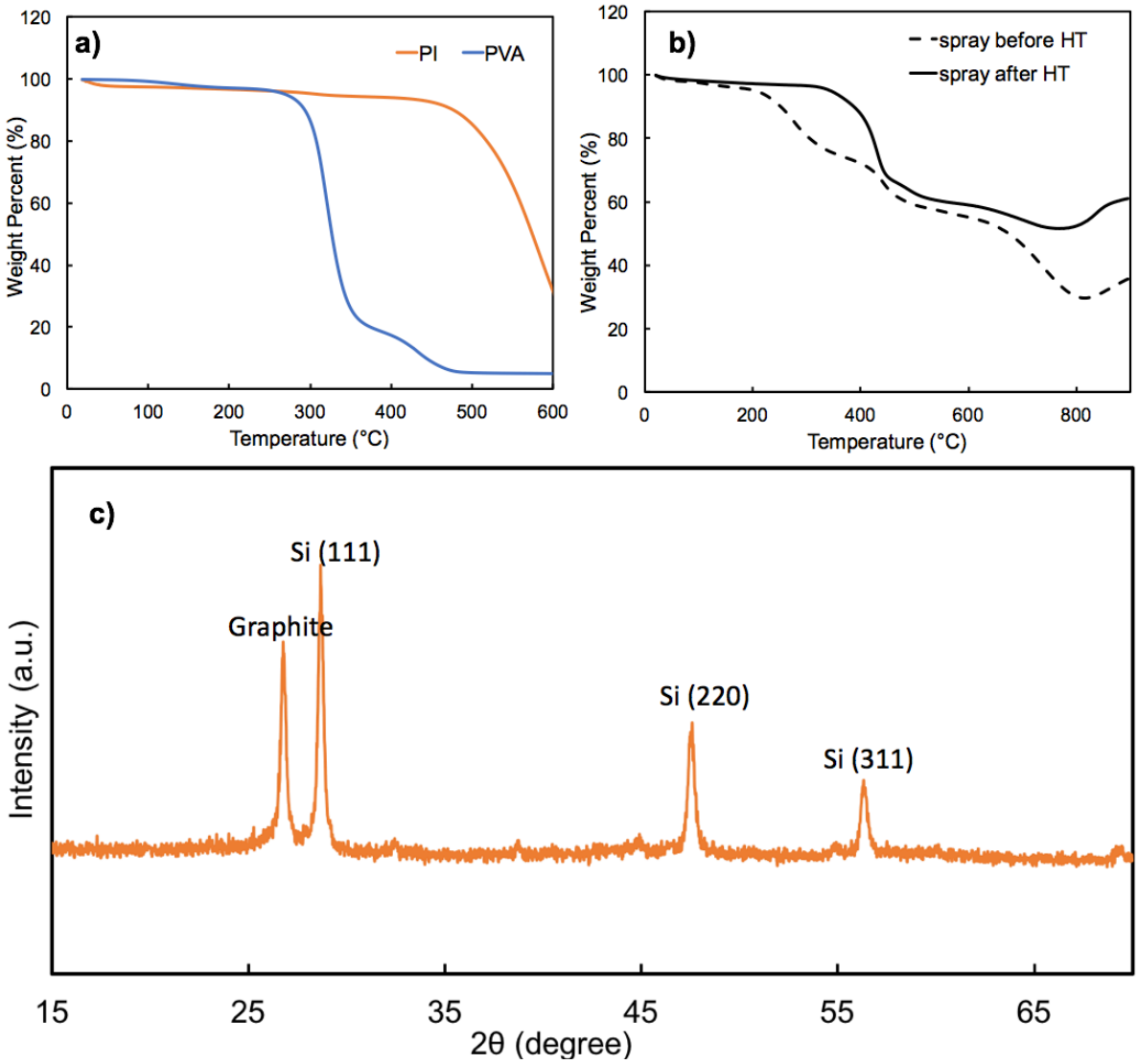

Fig. 2.4. TGA of **a)** PI and PVA **b)** disc before and after thermal annealing. **c)** XRD pattern of Si/Gr/Grpht anode after thermal annealing.

2.3.3 Graphite Anodes with Modifications

After thermal annealing, electrode Si content increases from 30% to 50% due to removal to PVA (Figure. 2.4b). Surface morphology of graphite anode with Si/Gr hybrid composites (Si/Gr/Grpht) can be seen from **Figure. 2.3c**. Note that Si/Gr and graphite distribute evenly and is not porous. However, after heat treatment, holes come up onto electrode surface indicates electrode's porous nature after excess binder removal (Figure. 2.3d). Si crystalline structure is well retained after thermal treatment, which is characterized by XRD (Figure. 2.4c). The XRD

pattern shows Si characteristic peaks corresponding with (111), (220) and (311) planes of Si [25]. However, PVA removal triggers concerns about system's packing density and active materials contact. Cross section SEM image (Figure. 2.3e) corroborates previous hypothesis of active materials disconnection. SiNPs' low self-conductivity leads to their heavy dependence on conductive agent, in this case, graphene, in order to involve in interactions. Besides decrease in inner conductive pathways, porous electrode surface results in a highly open structure which leads to unnecessarily huge silicon exposure to electrolyte solution. The red arrow points to place that active materials lose contact. In order to alleviate this problem, calendering is performed before thermal treatment and this step increases electrode density from 0.6g/cc to 0.8 g/cc, resulting into a denser structure with appropriate void spaces exist, pointed by red arrow (Figure. 2.3f).

Compression cannot fix another potential issue caused by anode's highly open surface. Even though inner void space improves system's strength in relaxing strain during lithiation/de-lithiation, SiNPs settled on electrode surface expose directly to electrolyte will trigger side reactions that aggravate Si waste and capacity drop at initial cycling stage. Besides, those SiNPs expand and contract severely without limitations at electrode surface directions, in this case, volume changes will lead to cracks and electrode degradation is highly possible to happen. Moreover, cracks will cause continuous SEI formation. Thick SEI layer will block Li^+ transport and intensify instable cycle retention gradually. Thus, we come up with idea to add extra graphene thin layer on top to cover whole electrode surface, aiming to create a stable SEI layer between electrolyte and graphene, instead of silicon, which largely avoids SiNPs wasting at initial stage. In other words, graphene is a protection layer of beneath electrode physically and electrochemically. **Figure. 2.3g** is cross section of graphene sprayed on copper substrate, with loading from 0.04 mg cm^{-2}, 0.06 mg cm^{-2} to 0.1 mg cm^{-2} for 1min, 2min and 3min spray time

respectively. Cracks can be observed when graphene loading is at 0.04 mgcm^{-2} and thus weakens graphene's geometric merit and meanwhile allows electrolyte leaking through, which also leads to irreversible SEI formations. Smooth graphene layer appears when loading is higher than 0.06 mg cm^{-2}. **Figure. 2.3h** shows the cross section of the uncompressed electrode with graphene layer on top after thermal annealing and a gap between protection layer and electrode surface can be clearly observed. Fortunately, with compression in advance, graphene layer is able to attach on smooth electrode tightly (Figure. 2.3i). With both modifications, we believe a mechanically and chemically stable architecture is built which will be proved later.

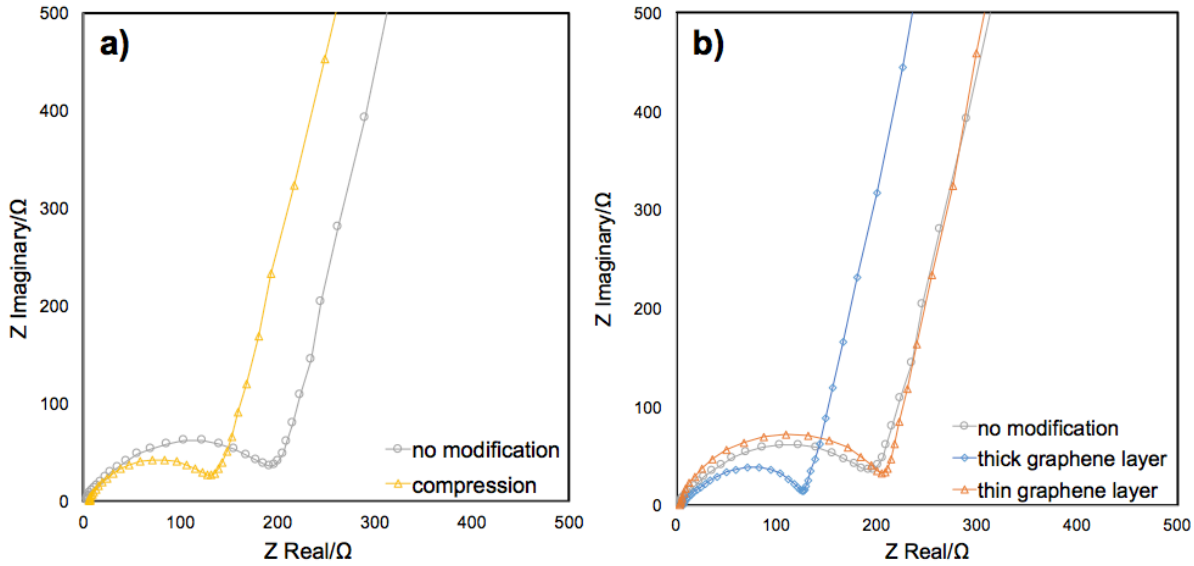

Fig. 2.5. Electrochemical impedance spectroscopy profiles of **a)** disc with no modifications, disc with thin graphene layer (0.04 mgcm-2) and disc with thick graphene layer (0.06 mgcm^{-2}) **b)** disc with no modifications and disc after calendared.

2.3.4 Creating Conductivity

Improvements of battery's electrochemical performances confirmed by Electrochemical impedance spectroscopy (EIS). EIS is performed on two sets of half-cells: either with or without compression or with diverse graphene layer thicknesses. Semicircle at high frequency

region represents electrode inner charge transfer impedance and the sloped line at lower frequency is measurement of Li-ion diffusivity [26]. Inner resistance has more than 25% decrease through slight calendaring disk from 0.6 g/cc to 0.8 g/cc without hindering Li-ion diffusivity from **Figure. 2.5a**. By calendering disc, more inner conductive pathways are created because of reconnection between active materials. Moreover, according to Figure. 2.5b, disc without graphene layer and discs with different graphene layer thickness show almost same Li^+ diffusivity, which implies that extra protection layer with less than 0.06 mg cm^{-2} graphene loading will not block Li^+ movement during intercalation/de-intercalation process and this can be explained by chemistry nature of lithium ion as one of the smallest charged ion radii on earth [27]. Inner resistance is reduced by around 40% by adding 0.06 mg cm^{-2} graphene layer due to graphene's superior conductivity (Figure. 2.5b). However, graphene layer with loading of 0.04 mg cm^{-2} gives very similar profile as that of disc without modifications that because as more graphene is deposited onto electrode, we can expect more contacts in between. Problem come with thick graphene layer is its effect on specific capacity and volumetric energy reduction so that we pick 0.04 mg cm-2 graphene loading for further cycling test, instead of thickest graphene coating.

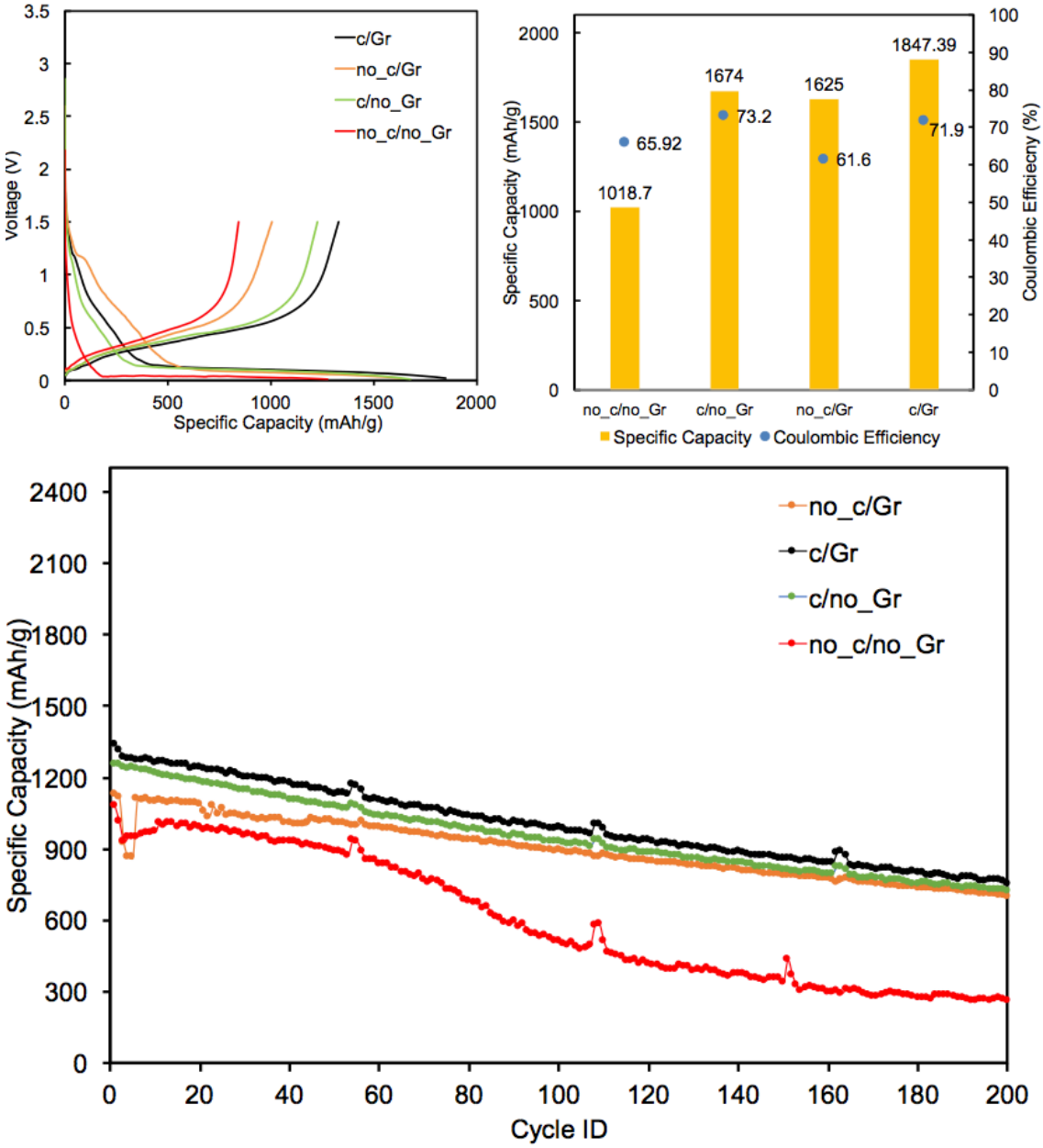

Figure 2.6. a) capacity-voltage profiles of no_c/no_Gr, c/no_Gr, c/Gr, no_c/Gr. **b)** 1st cycle discharge specific capacity and coulombic efficiency of no_c/no_Gr, c/no_Gr, no_c/Gr and c/Gr. **c)** galvanostatic discharge/charge profiles of no_c/no_Gr, c/no_Gr, no_c/ Gr and c/Gr.

2.3.5 Electrochemical Testing of Modified LIB Anode

Four types of half-cells are prepared and are representative all possible modification combinations, including: without both compression and graphene layer (no_c/no_Gr); without compression and additional graphene layer (no_c/Gr); compression with no graphene layer

(c/no_Gr) and compression with additional graphene layer (c/thin_Gr). When graphene loading lower than 0.06mgcm^{-2}, protection layer has too many defects **Figure. 2.3i** and has potential to expose Si/Gr nano composites to electrolyte so that all graphene layer is fixed at 0.06mgcm^{-2} to avoid these potential issues. All capacities mentioned below are referred to specific capacity, which include total electrode weight, except from copper substrate into consideration. **Figure. 2.5a** depicts capacity-voltage profiles at 420 mAhg^{-1} for all cases. SEI formation is a morphology-dependent process and electrolyte solution starts decomposition earlier when electrode surface show more defects [27]. When the disc does not go through any modification, no_c/no_Gr discharge curve shows the largest slope and ohmic potential drop (IR drop), which elucidates the fact that electrolyte starts deposition at the earliest time due to its highly open structure and large electrode inner resistance comparing with other cases. The highly open structure leads to more Li^+ waste for irreversible SEI formation. Moreover, it has lowest specific capacity (Figure. 2.5b), which is a proof of not only irreversible capacity losses from SEI formation, but also shortage of inner conductive pathways for Li ions due to the loose structure after thermal annealing. The second largest irreversible capacity loss is c/no_Gr, the case that anode goes through compression but does not have graphene protection layer. We can see Coulombic efficiency is improved a lot and this implies that after being compressed, electrode surface becomes smoother and contact between active materials and electrolyte decreases for less defects on electrode surface. Furthermore, electrode geometry is more densely packed thus specific capacity increases by 650 mAh/g comparing to no_c/no_Gr case, which is beneficial from more inner conductive pathways. Besides that, first cycle Coulombic efficiency is slightly improved. For cases Si/Gr/Grpt covered by robust and conductive graphene layer (no_c/ Gr, c/Gr), additional plateaus appear at around 1.2V, which represent reactions between graphene and electrolyte [28]. Different from Si's low working potential, graphene starts to store Li^+ at a much higher potential, higher than 0.5V. Ohmic potential drops

are improved in these cases because extra conductive graphene layers on top reduces inner resistance effectively and electrochemical reactions between graphene and electrolyte prevents those between silicon nanoparticles and electrolytes. Reversible capacity is thus reserved.

Detailed specific capacity and coulombic efficiency comparisons among these cases further confirm our expectations about modifications' effectiveness on battery electrochemical performances. First, as stated before, specific capacity rises around 650 mAh/g by compression and adding graphene layer on electrode surface gives us similar effect. These two approaches boost cells' energy storage ability through reducing electrode inner resistance by either increasing interconnected conductive pathways to facilitate Li-ion mobility or fabricating stable SEI layer that reserve system's capacity. From literatures, graphene-only anodes always show a low coulombic efficiency and larger potential windows are required [28, 30-31], which is graphene intrinsic drawback caused by high surface area and disables it as energy storage material [29]. This fact explains c/thick_Gr has the lowest coulombic efficiency. Combination of these modifications could be solution and cells exhibit highest capacity and coulombic efficiency (~71%) that in between 66% and 73%.

Cycle retention profiles (Figure. 2.5c) illustrate systems' ability to maintain geometric integrity and provide Li^+ conductive pathways in long-term charge/discharge process. System with no modification shows severe decay as expectation, which mainly comes from continuous fresh SiNPs exposures to electrolyte during cycling, in other word, continuous SEI formation. This profile has very similar trend with that of bare Si system, which starts high and drops drastically after several cycles when Si oxidized layer cannot hold the strain from Li^+ intercalation and de-intercalation. Inner void spaces that we made deliberately could not function properly in this case, instead, aggravate shortage in activations site and conductive pathways issues.

C/no_Gr, no_c/Gr and c/Gr show much more improved cycle retentions and have 720.3 mAh g^{-1}, 702.5 mAh g^{-1} and 770.2 mAh g^{-1} respectively after 200 cycles at 1.26 Ah g^{-1}, and these retained capacities are much higher than graphite's theoretical capacity, which is around 372 mAh g^{-1} at full lithiation. The smart architecture with inner void spaces is proved to be able to maintain stable system integrity and provide adequate conductive pathways simultaneously. Combination of two modifications (c/Gr) delivers highest specific capacity. Initially, graphene layer provides conductivity that allow Li-ion move through faster and protective SEI is formed due to graphene electrolyte interactions. As charge/discharge processes prolong, silicon nanoparticle expands themselves, filling themselves in void spaces inside the anode structure and system gradually becomes more packed, with pressure from SEI layer on top.

2.4 Conclusion

In this work, Si/Gr nano composites, excess binder, conductive agents and graphite are directly deposited on copper substrate via air-assisted, water-based electrospray method, which eliminates extra drying step in traditional slurry preparation, time saving, controllable and non-toxic. Thermal annealing for binder removal effectively creates electrode inner void spaces which accommodate SiNPs volume expansion and facilitate faster electrolyte penetration. Out of concerns for nano structured electrode's intrinsic drawbacks, such as high surface area, strong inner resistance and weak conductivity, calendering and adding graphene layer are performed to further modify anode morphology by offering more activation sites and conductive pathways. Either compression or graphene layer gives cell higher specific capacity and better cycle retention at 1.26 Ah g^{-1} and combination of compression and graphene layer with loading of 0.06 mg cm^{-2} delivers the best result. We engineer Silicon/Carbon electrode matrix with modifications and prove that optimized system with proper amount of inner void spaces, graphene layer loading and extent of compression is very promising in future

commercialization with good cycle retention and more than doubled capacity of that of graphite after long cycles. In conclusion, this study is achieved with simple and non-toxic process and suitable for scaling up in future. Si/Gr/Grpt system with appropriate modifications is anode system that can support development of next-generation, high-capacity, long-cycle and portable Li-ion battery.

Conflict of interest

There are no conflicts to declare.

Acknowledgements

This work was partly supported by Hyundai Motors (Cornell OSP No. M019140) and DJ Semichem (Cornell OSP NO. M019122). All the material characterizations were obtained via facilities at the Cornell Center for Materials Research (part of NSF MRSEC Program, Grant DMR 1120296).

References

[1] G. Shoorideh, B. Ko, A. Berry, M.J. Divvela, Y.S. Kim, Z. Li, P. Patel, S. Chakrapani, Y.L. Joo, Harvesting Interconductivity and Intraconductivity of Graphene Nanoribbons for a Directly Deposited, High-Rate Silicon-Based Anode for Li-Ion Batteries. ACS Applied Energy Materials. 1 (2018) 1106-1115. doi:10.1021/acsaem.7b00228.

[2] J. Hassoun, F. Bonaccorso, M. Agostin, M. Angelucci, M.G. Betti, R. Cingolani, M. Gemmi, C. Mariani, S. Panero, V. Pellegrin, B. Scrosati, An Advanced Lithium-Ion Battery Based on a Graphene Anode and a Lithium Iron Phosphate Cathode. Nano Letters**.** 14 (2014) 4901-4906. doi:10.1021/nl502429m.

[3] B.L. Hu, F. Wu, C. Lin, A.N. Khlobystov, L. Li, Graphene-modified LiFePO4 cathode for lithium ion battery beyond theoretical capacity. Nature Communications. 4 (2013). doi:10.1038/ncomms2705.

[4] H.Z. Zhang, Q.Q. Qiao, G.R. Li, S.H. Ye, X.P. Gao, Surface nitridation of Li-rich layered $Li(Li_{0.17}Ni_{0.25}Mn_{0.58})O_2$ oxide as cathode material for lithium-ion battery. Journal of Materials Chemistry. 22 (2012), 13104-13109. doi:10.1039/c2jm30989k.

[5] N.Y. Kim, C. Oh, J.Y. Kim, J.S. Kim, E.D. Jeong. J.S. Bae, J.K. Lee, High-Performance Li-Ion Battery Anodes Based on Silicon-Graphene Self-Assemblies. Journal of The Electrochemical Society. 164(2017) A6075-A6083. doi: 10.1149/2.0101701jes.

[6] S.D. Beattie, D. Larcher, M. Morcrette, B. Simon, J. Tarascon, Si Electrodes for Li-Ion Batteries—A New Way to Look at an Old Problem. Journal of The Electrochemical Society. 155 (2018) A158-A163. doi:10.1149/1.2817828.

[7] H. Tang, J. Zhang, Y. Zhang, Q. Xiong, Y. Tong, Y. Li, X.L. Wang, C.D. Gu, J. Tu, Porous reduced graphene oxide sheet wrapped silicon composite fabricated by steam etching for lithium-ion battery application. Journal of Power Sources. 286 (2015) 431-437. doi:10.1016/j.jpowsour.2015.03.185.

[8] A. Casimir, H. Zhang, O. Ogoke, J.C. Amine, J. Lu, G. Wu, Silicon-based anodes for lithium-ion batteries: Effectiveness of materials synthesis and electrode preparation. Nano Energy. 27 (2016) 359-376. doi:10.1016/j.nanoen.2016.07.023.

[9] K. Feng, W. Ahn, G. Lui, H.W. Park, A.G. Kashkooli, G. Jiang, X. Wang, X. Xiao, Z. Chen, Implementing an in-situ carbon network in Si/reduced graphene oxide for high performance lithium-ion battery anodes. Nano Energy. 19 (2016), 187-197. doi:10.1016/j.nanoen.2015.10.025.

[10] E. Peled, S. Menkin, Review—SEI: Past, Present and Future. Journal of The Electrochemical Society. 164 (2016) A1703-1719. doi:10.1149/2.1441707jes.

[11] B. Wang, X. Li, X. Zhang, B. Luo, M. Jin, M. Liang, S.A. Dayeh, X.T. Picraux, L. Zhi, Adaptable Silicon–Carbon Nanocables Sandwiched between Reduced Graphene Oxide Sheets as Lithium Ion Battery Anodes. ACS Nano. 7 (2013) 1437-1445. doi:10.1021/nn3052023.

[12] Z. Wen, G. Lu, S. Mao, H.J. Kim, S. Cui, K. Yu, X. Huang, P.K. Hurley, O. Mao, J. Chen, Silicon nanotube anode for lithium-ion batteries. Electrochemistry Communication. 28 (2013) 67-70. doi:10.1016/j.elecom.2013.01.015.

[13] Y. Zhang, N. Du, S. Zhu, Y. Chen, Y. Lin, S. Wu, D. Yang, Porous silicon in carbon cages as high-performance lithium-ion battery anode Materials. Electrochimica Acta. 252 (2017) 438-455. doi:10.1016/j.electacta.2017.08.038.

[14] N. Liu, Z. Lu, L. Zhao, M.T. Mcdowell, H. Lee, W. Zhao, Y. Cui, A pomegranate-inspired nanoscale design for large-volume-change lithium battery anodes. Nature Nanotechnology. 9 (2014) 187-192. doi:10.1038/NNANO.2014.6.

[15] J.K. Lee, K.B. Smith, C.M. Hayner, H.H. Silicon nanoparticles–graphene paper composites for Li ion battery anodes. Chemical Communications. 46 (2010) 2025-2027. doi:10.1039/b919738a.

[16] M.H. Park, M.G. Kim, J. Joo, K. Kim, J. Kim, S. Ahn, Y. Cui, J. Cho, Silicon Nanotube Battery Anodes. Nano Letters. 9 (2009) 3844–3847. doi:10.1021/nl902058c.

[17] L. Hu, H. Wu, S.S. Hong, L. Cui, J.R. Mcdonough, S. Bohy, Y. Cui, Si nanoparticle-decorated Si nanowire networks for Li-ion battery anodes. Chemical Communications. 47 (2011) 367-369. doi:10.1039/C0CC02078H.

[18] J. Luo, X. Zhao, J. Wu, H.D. Jang, H.H. Kung, J. Huang, Crumpled Graphene-Encapsulated Si Nanoparticles for Lithium Ion Battery Anodes. J. Phys. Chem. Lett. 3 (2012) 1824–1829. doi:10.1021/jz3006892.

[19] P. Lian, X. Zhu, S. Liang, Z. Li, W. Yang, H. Wang, Large reversible capacity of high quality graphene sheets as an anode material for lithium-ion batteries. Electrochimica Acta. 55 (2010) 3909-3914. doi:10.1016/j.electacta.2010.02.025.

[20] W. Lv, Z. Li, Y. Deng, Q. Yang, F. Kang, Graphene-based materials for electrochemical energy storage devices: Opportunities and challenges. Energy Storage Materials. 2 (2016) 107-138. doi:10.1016/j.ensm.2015.10.002.

[21] Wang, H.; Li, X.; Baker-Fales, M.; Amama, P. B. 3D graphene-based anode materials for Li-ion batteries. *Current Opinion in Chemical Engineering* **2016**, 13, 126-132

[22] L. Fei, S.H. Yoo, R.A.R. Villamayor, B.P. Williams, S.Y. Gong, S. Park, K. Shin, Y.L. Joo, Graphene Oxide Involved Air-Controlled Electrospray for Uniform, Fast, Instantly Dry, and Binder-Free Electrode Fabrication, ACS Appl. Mater. Interfaces. 9 (2017) 9738–9746. doi:10.1021/acsami.7b00087.

[23] J. Lee, B. Ko, J. Kang, Y. Chung, Y. Kim, W. Halim, J.H. Lee, Y.L. Joo, Facile and scalable fabrication of highly loaded sulfur cathodes and lithium–sulfur pouch cells via air-controlled electrospray, Mater. Today Energy. 6 (2017) 255–263. doi:10.1016/j.mtener.2017.11.003.

[24] X. Liu, X. Zhu, D. Pan, Solutions for the problems of silicon–carbon anode materials for lithium-ion batteries. Royal Society Open Science. 5 (2018). doi:10.1098/rsos.172370.

[25] X. Gao, J. Li, Y. Xie, D. Guan, C. Yuan, A Multilayered Silicon-Reduced Graphene Oxide Electrode for High Performance Lithium-Ion Batteries. ACS Applied Materials & Interfaces. 7 (2015) 7855-7862. doi:10.1021/acsami.5b01230.

[26] N. Li, S. Jin, Q. Liao, H. Cui, C. Wang, Encapsulated within graphene shell silicon nanoparticles anchored on vertically aligned graphene trees as lithium ion battery anodes. Nano Energy. 5 (2014) 105-115. doi:10.1016/j.nanoen.2014.02.011.

[27] H. Sun, A. Varzi, V. Pellegrini, D. Dinh, R. Raccichini, A.D. Rio-Castillo, M. Prato, M. Colombo, R. Cingolani, B. Scrosati, S. Passerini, F. Bonaccorso, How much does size really matter? Exploring the limits of graphene as Li ion battery anode material. Solid State Communications. 251 (2017) 88-93. doi: 10.1016/j.ssc.2016.12.016.

[28] G. Wang, X. Shen, J. Yao, J. Park, Graphene nanosheets for enhanced lithium storage in lithium ion batteries. Carbon. 47 (2009) 2049-2053. doi:10.1016/j.carbon.2009.03.053.

[29] Q. Cheng, Y. Okamoto, N. Tamura, M. Tsuji, S. Maruyama, Y. Matsuo, Graphene-Like-Graphite as Fast-Chargeable and High-Capacity Anode Materials for Lithium Ion Batteries. Scientific Reports. 7 (2017). doi:10.1038/s41598-017-14504-8.

[30] R.P. Luo, W.Q. Lyu, K.C. Wen, W.D. He, Overview of Graphene as Anode in Lithium-Ion Batteries. Journal of Electronic Science and Technology**.** 16 (2018) 57-68. doi: 10.11989/JEST.1674-862X.6032519.

[31] E. Yoo, J. Kim, E. Hosono, H. Zhou, T. Kudo, I. Honma, Large Reversible Li Storage of Graphene Nanosheet Families for Use in Rechargeable Lithium Ion Batteries. Nano Letters. 8 (2008) 2277-2282. doi:0.1021/nl800957b.

Chapter 3

Directly Deposited Si/Graphene Oxide Lithium-ion Battery Anode and Further Study on their Size Ratio Effects

3.1 Introduction

Rechargeable batteries take a predominant role in current energy market as the main power source provider and clean, sustainable solution for consumer electronics and fast-growing electric vehicle markets [1,2]. However, batteries' development speed is not comparable with that of electronic devices development and does not follow electronics Moore's Law [2]. Even though lithium-ion batteries (LIB), as the popular rechargeable batteries, offer much higher energy and power densities comparing with other kinds of commercialized batteries [3], there still exists many drawbacks that hinder LIB fulfilling more and more requests from current market. Traditional graphite anode material is the part that needs a technical revolution on urge because as it was in use since its first invention in 1991, its theoretical capacity was reached by that time [4]. There's no significant capacity breakthrough during these nearly 30 years and the relatively low theoretical capacity (372 mAh/g) cannot reach the needs for many energy applications, especially electric vehicles market [5]. Silicon is one of the most promising candidates as next-generation LIB anode materials due to its natural abundance, low working potential and more than 10 times higher theoretical capacity (4200 mAh/g) than that of graphite, [6,7]. However, as a lithium ion host, Si goes through huge volume expansion/contraction, up to 300% during lithium insertion/extraction and this will cause potential issues such as material pulverization, electrode degradation and furthermore, continuous solid electrolyte interface (SEI) formation [1]. Lack of system integrity during LIB charge/discharge process will gradually deteriorate battery's electrochemical performance and makes retaining good cycle life and capacity become very challenging [8,9]. Researchers found out that Si/C composites

anode system can effectively circumvent these problems and graphene and graphene oxide are some of the most mentioned carbon materials involved in these systems [10-14].

First successfully prepared in 2004 by Novoselov and co-workers [15], graphene has attracted researchers' tremendous attentions these years. This two-dimensional, single-atom-thick layer structured carbon material immerses in wide-range of industrial applications due to its superior properties such as chemical stability, strong mechanical strength and robustness, electrical conductivity, high thermal tolerance and large specific surface area [16-19]. These properties also qualify graphene as a suitable substrate to host active materials and promising candidate of next-generation LIB electrode material [20]. During recent years, graphene has been produced through several ways, either physically or chemically. These approaches include mechanical exfoliation of graphite using scotch tape [21], liquid phase production and chemical vapor deposition [22-24]. Instead of technical difficulties appeared in graphene synthesis and quality control, graphene oxide (GO), the functionalized graphene with oxygen functional group [25] and also commonly used as precursor of graphene production [21], can nowadays be simply produced through modified Hummers Method [26]. Due to these functional groups, GO has more structural defects comparing with pristine graphene and thus lose some electrical conductivity [27]. However, these functional groups of large varieties, including carbonyl (C=O), carboxyl (C-OOH), hydroxyl (C-OH) and epoxy (C-O-C) groups also enable GO properties graphene does not own, such as stable aqueous suspension, enhanced chemical activity and tunable optical transmittance [21,25,27]. Especially GO's good solvent dispersibility and colloidal stability in water can be very crucial for applications with water solvent involved [28]. There are several approaches, either thermally or chemically to reduce GO into reduced graphene oxide (rGO) and rGO has semiconductor or even semimetal property close to that of graphene depends on extent of these reduction [27].

With those exceptional qualities stated before, it is not surprising that not only graphene, graphene oxide also gains many research interests these year, especially in energy storage applications. Researchers explore GO's properties as energy storage materials and found that GO that goes through various extent and approaches of reduction shows comparable capacity with pristine graphite, which is traditional lithium ion battery (LIB) anode materials and stable cycle retention [29]. However, GO is more remarkable as electrode structural material and frequently involved into Silicon included composite LIB anode systems, including bilayer Si/RGO membrane [17], 3D Silicon/rGO/CNT composite nanostructure [11,12] and Silicon/CNF composite wrapping with rGO protection layer [13]. Moreover, one of our previous works [14] also takes use rGO to form rGO/Silicon layered structure LIB anode system via air-controlled electrospray method. All of these works corroborate that these composite systems have longer cycle life and much improved specific capacity comparing with that of traditional graphite anode and these results are benefited by rGO serving as both conductive agents for more efficient silicon utilization and protection interlayers for relaxing stress from silicon volume expansion. As discussed before, GO has noticeable stable colloidal suspension in water solvent due to its unique structure composed of hydrophobic basal and hydrophilic edges and can thus deposited onto substrate and form thin conductive films through simple means such as drop-casting, spray and spin-coating [1]. Inspired by this idea, our group's previous work thus stands out because of proper utilization of GO's liquid crystal property in electrode fabrication via air-controlled electrospray method, which is a low cost, water-based and nontoxic process that no needs for extra drying step [14].

In our previous work [14], we have shown that air-controlled electrospray method is a facile, nontoxic and efficient electrode preparing approach, which could result in a layer-by-layer and

binder-free Si/GO nanostructured LIB anode system of much improved cycle retention comparing with that of disc produced through conventional slurry coating. In this study, we are trying to further optimize this advanced Si/GO system by exploring size effects from different active materials. We selected GO (KSICO Inc.) of different sizes (<5μm, 10μm, 40μm) in addition to both silicon nanoparticles (SiNPs) (30-50nm) and ball milled silicon micro-particles (mSiMPs) (around 0.3μm) and directly deposited these active materials onto copper collector via water-based, air-controlled electrospray method. Resulting electrodes show good adhesion, uniform active materials distribution and layered electrode structure, which proves that this simple approach is applicable for various solution conditions and we can then have understanding of how different sizes and shapes of conductive agents (rGO) and active materials (Si) affect electrode system packing and further affect battery performance in terms of long-term cycling ability and high-rate capability.

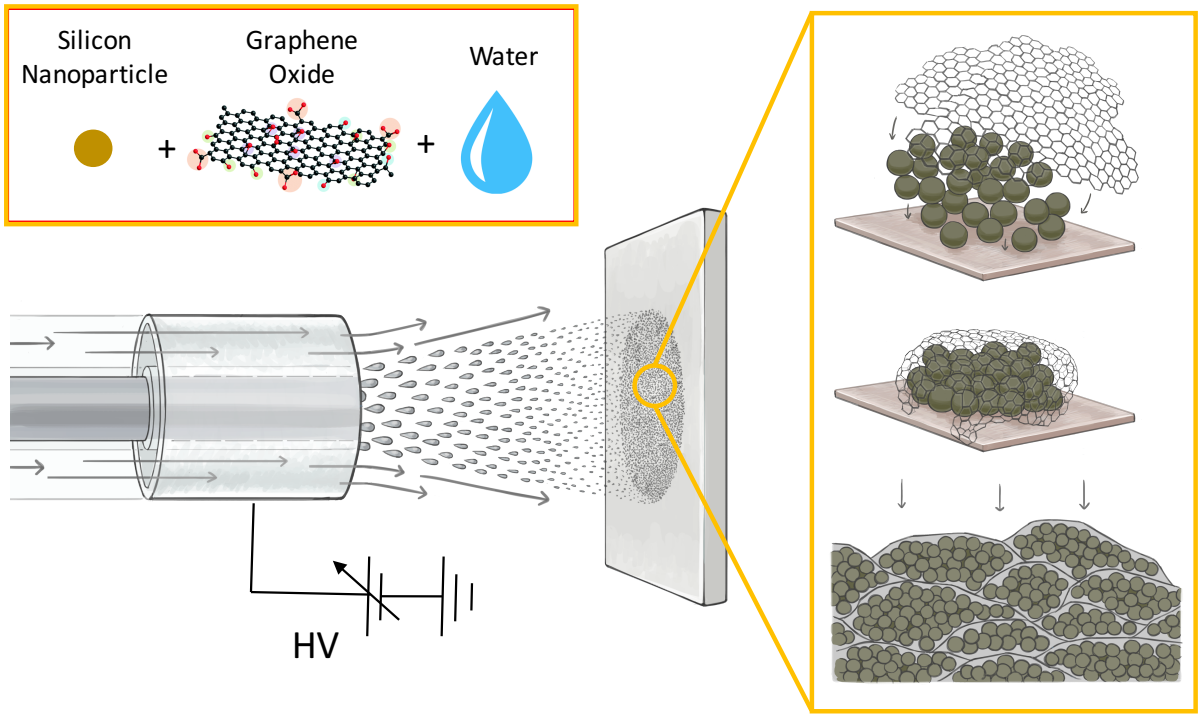

Fig. 3.1. Schematic illustrations of air-controlled electrospray process for Si/GO nanostructured electrode preparation.

3.1 Experimental Section

3.2.1 Preparation of GO-only Electrodes

3mL GO solution (KISCO, 2wt% GO sheets) was typically collected for GO-only electrodes preparation via air-controlled electrospray method. Harvard Apparatus PHD 2000 infusion syringe pump was taken use with a coaxial nozzle set which is composed of an inner 12G needle and an outer 17G needle. For air-controlled electrospray, nozzle tip was set 20cm from current collector with copper disc attached on it in addition with 25 kV working voltage, 25 psi air pressure and 0.05 mL min^{-1} infusion rate. This setting was fixed for each trail with GO solution of various sizes, ranging from <5μm, 10μm to 40μm. Graphene oxide flakes were thus directly deposited onto copper collector and the target active materials amount was around 2.0mg per disc (around 1.1mg cm^{-2}). In order to turn GO into conductive rGO, pre-sprayed electrodes were thus thermal annealed at 400˚C in N_2 atmosphere for 2 hours in furnace (MTI Tube Furnace) at ramp of 5˚C min^{-1}.

3.2.2 Preparation of GO/Si, rGO/Si Electrodes

Heat treatment (Mellen Furnace) was done on ball milled SiMP at 1000ºC in Ar for 1 hour at ramp of 5 ºC min^{-1}. This extra step was done with the purpose of eliminating extra contaminations and oxidization occurred during IPA/DI milling. After that, same air-controlled electrospray instrument was employed for Si/GO electrodes preparations. 1.0g deionized waster was first mixed with 0.1g silicon nanoparticles (US Research Nanomaterials Inc., 98+%, 30-50nm) or silicon micro-particles (DJ Semi-Chem Inc.) and the silicon paste was sonicated for 1 hour (Qsonic). Different amounts of GO solutions were then added according to their different mass reduction results in order to achieve electrodes of consistent rGO: SiNP ratio (4:6) and further, fair electrochemical performance comparison. Solution was then sonicated (Qsonic) for another 1 hour before spraying. Solutions involved ball milled silicon micro-

particles instead of SiNPs as active materials were stirred overnight for better dispersion. Working conditions were same with GO-only electrode preparation except for infusion rate, which decreased from 0.05mL/min to 0.035mL/min. Moreover, GO/SiNP and GO/mSiMP were thermally annealed at 400˚C in N_2 atmosphere for 2 hours in furnace (MTI Tube Furnace) in order to get rGO/SiNP and rGO/mSiMP LIB anodes.

3.2.3 Characterization

The surface and cross-section morphologies of nanostructured rGO/SiNP and rGO/mSiMP electrodes were characterized by scanning electron microscopy (SEM, LEO 1550 FESEM). The electrode elementary distribution was determined by energy dispersive X-ray (EDS, LEO 1550). Functional group changes were shown by Fourier transformed infrared (FTIR) spectrum which measured by Bruker Vertex V80V Vacuum FT-IR system. Silicon and GO/rGO ratio was illustrated by thermogravimetric analysis (TGA, TA Instrument Q500) which conducted from 20°C to 900°C at ramp of 10°C min^{-1} under air atmosphere. The surface area and porosity of these GO/Si composite systems were indicated by BET N_2 adsorption/desorption method carried out through Micromeritics Gemini VII. Furthermore, silicon's crystalline structure and X-ray diffraction patterns of graphene oxide before and after thermal annealing were investigated through a D8 powder diffractometer (XRD, Bruker).

Electrochemical characterizations were operated on 2032R coin cell. Prepared rGO/SiNP and rGO/SiMP electrodes were stored in vacuum oven at 100ºC at least one day before cell assembly to avoid ambient moisture. After drying step, rGO/Si electrodes were used as anodes of half-cell and lithium foil as counter electrode. 1M solution composed of $LiPF_6$ dissolved in mixture of ethylene carbonate and dimethyl carbonate (50:50 wt/wt%) with 10 wt% fluoroethylene carbonate as additive was used as electrolyte for Si-based electrodes and

separator in between electrodes was polypropylene membrane (Celgard, USA). Cell assembly was performed in argon-filled glovebox with water and oxygen levels below 0.5 ppm. Galvanostatic charge/discharge process was tested under 0.01-1.5V voltage window at current density 0.18A g^{-1} for the first cycle and 1.26A g^{-1} for further cycles using BTSDA battery analyzer. Electrochemical Impedance Spectroscopy (EIS, PARSAT 4000, Princeton applied research) measurement was conducted with amplitude of 10 mV in frequency range 0.1 Hz – 100 kHz. Cycling capacities and current densities reported were calculated into specific capacities, which counts total weight of disc excluding copper substrate.

GO Lot.#	1	2	3
flake size (μm)	<5	10	40
mass reduction (%)	58.12	58.67	59.88
1st discharge capacity (mAh/g)	590.19	1011.04	451.32
1st charge capacity (mAh/g)	131.58	357.66	96.05
Coulombic efficiency (%)	22.29	35.38	21.28

Table 3.1. Three different GO flake size, mass reduction and 1st cycle electrochemical properties tested under 0.01-1.5V.

3.3 Results and Discussions.

3.3.1 GO-only Electrode Performance

We first investigate several GO's property as electrochemical materials in order to have basic understandings before its further application in composite systems. We have 3 different kinds of products, which have name sample name of Lot.01, S10 and s40 and correspond to lot number 1, 2 and 3 in table for convenience (original sample name will be kept used in further paragraphs). After being thermally annealed, three GO samples we pick all show mass reduction around 60% (Table 3.1) due to removal of functional groups and we assume GO-only electrodes now become more conductive rGO-only electrodes. We also tested at current rate of 0.1C in order to fully activate the electrodes and found various first cycle capacity and

coulombic efficiency. First, we notice that 1st cycle discharge capacities for these rGO anodes are all much higher than that of theoretical capacity of graphite, which may due to lithium intercalation with residual oxygen functional groups [30]. Moreover, from **Table 3.1** we can see that highest coulombic efficiency is only 35.28%, which results from the fact that capacity generated by Li^+ interaction with functional groups is irreversible. Electrochemical performances determine that graphene oxide is not a suitable energy storage material, however, it should be an electrode structural material to facilitate lithium ion movement and support electrode integrity due to those superior properties we introduce before. For convenience, we will name Lot.01, S10 and S40 GO as GO_05, GO_10 and GO_40 and those numbers indicate GO size.

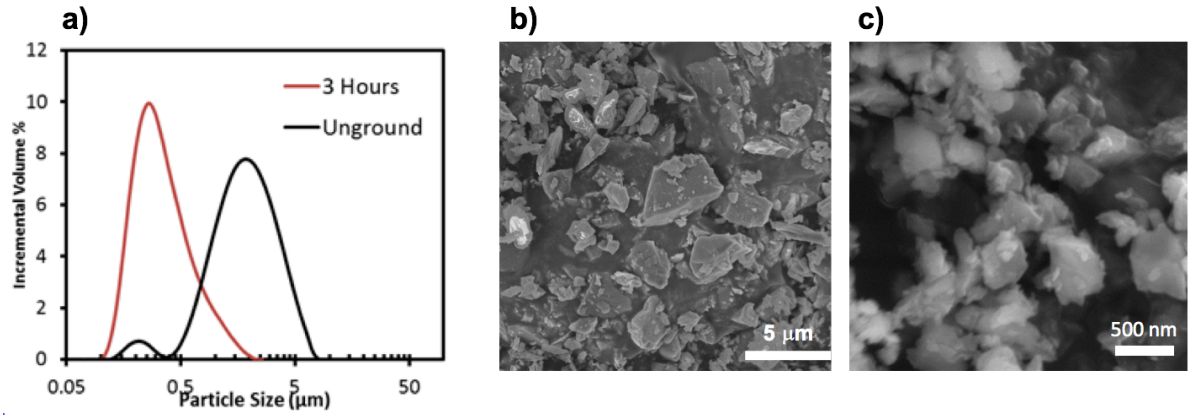

Fig. 3.2. a) Size distributions of SiMP and mSiMP, SEM images of **b)** SiMP **c)** mSiMP

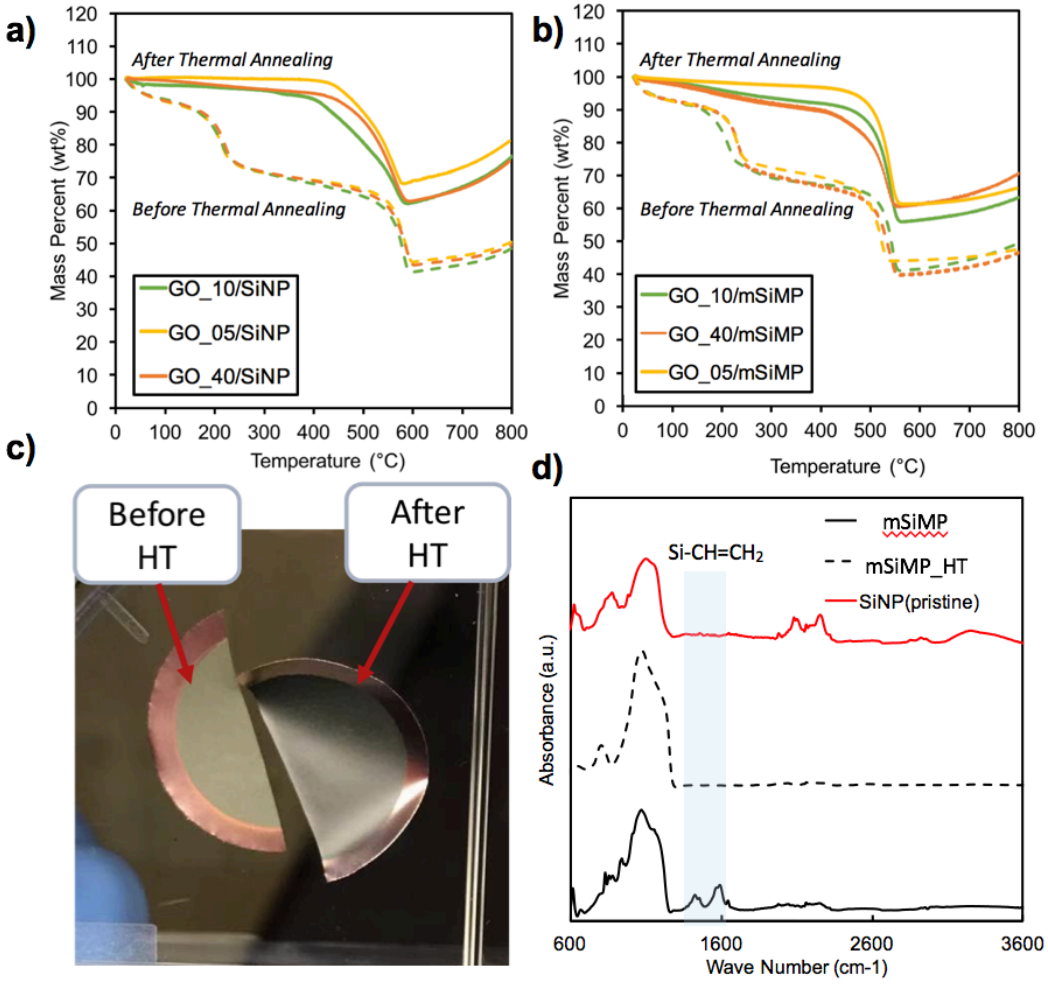

Fig. 3.3. TGA of **a)** GO/SiNP composite systems before thermal annealing (solid line) and after thermal annealing (dashed line) **b)** GO/SiMP composite systems before thermal annealing (solid line) and after thermal annealing (dashed line) **c)** electrode before and after thermal annealing **d)** FTIR for pristine SiNP, SiMP and heat treated SiMP.

3.3.3 rGO/SiNP and rGO/mSiMP

After having basic ideas about graphene oxide as anode materials, we now want to include SiNPs and mSiMPs into systems and optimize combination of silicon and GO with different flake sizes. mSiMPs are milled with DI water and IPA and average sizes are reduced to 0.3 μm, which can be seen from **Figure 3.2a**. Moreover, size changes can also be seen from SEM images (Figure 3.2 b and Figure 3.2c). In order to achieve fair comparisons, we control active

materials content in each system to be same. Heat treatment (1000ºC, 1hour, Ar) was conducted on our home-milled SiMP out of concerns for extra oxidation and contamination that potentially exist. **Figure 3.3 d** compares FTIR results of pristine SiNP, mSiMP and thermally treated mSiMP and light blue bar highlights the one of the main difference between these silicon particles. Heat treatment effectively removes additional functional groups that created during ball milling process and help us in avoiding potential confusions related to side reactions (We use mSiMP to represent mSiMP_HT in further paragraphs for convenience). **Figure 3.3 a** and **Figure 3.3 b** illustrate TGA results of total 6 conditions: Lot.01 GO and SiNP system (GO_05/SiNP), S10 graphene oxide and SiNP system (GO_10/SiNP), S40 graphene oxide and SiNP system (GO_40/SiNP), and similar for GO and mSiMP systems. Solid lines and dashed lines represent electrode composition before and after thermal annealing respectively. After being thermal annealed, solid-line profiles have one plateau less than that of dashed-line profiles due to removal of most functional groups and silicon contents increase from 40% to around 60%. Furthermore, disc goes through evident color change and displays grey metallic luster (Figure 3.3c) which is under our expectation due to the fact that GO can have semi-metal properties after reduction. Moreover, there's no detachment issue for this binder-free system after going through thermal annealing, which verifies GO's ability in assisting active materials adhesion.

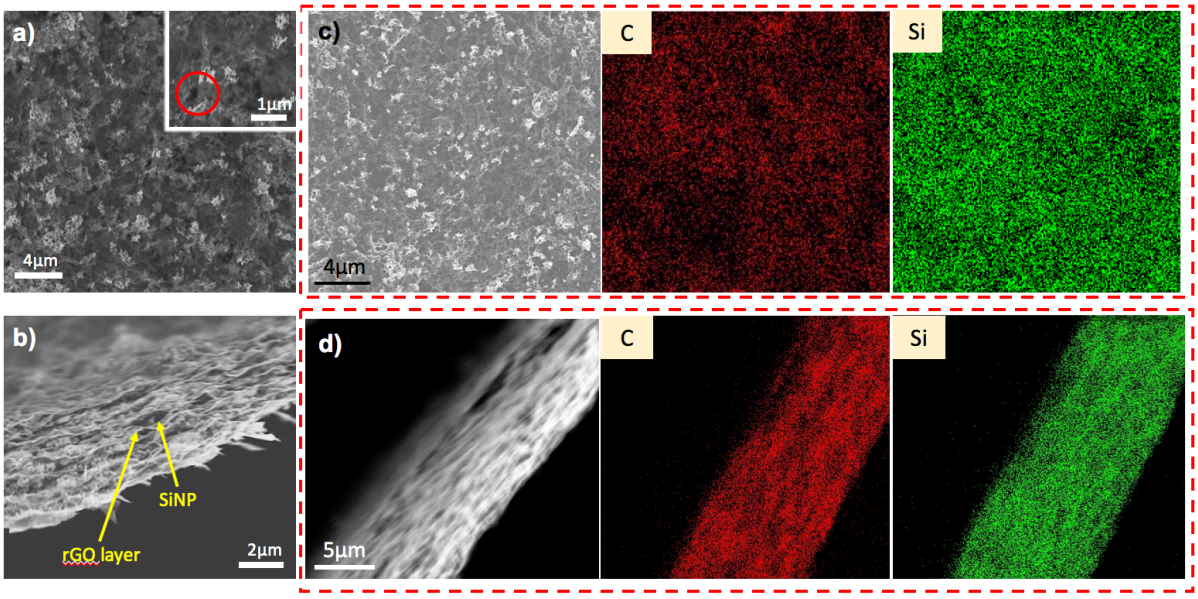

Fig. 3.4. Scanning electron microscopy image of rGO_05/SiNP electrode **a)** surface morphology **b)** cross-section morphology. Energy dispersive X-ray image of rGO/SiNP electrode **c)** surface elementary distribution **d)** cross-section elementary distribution.

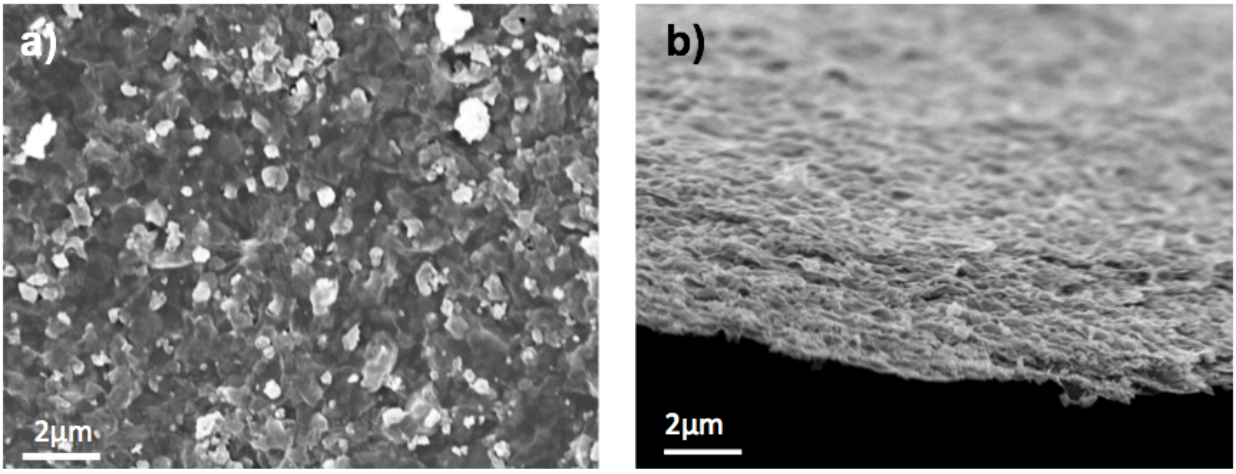

Fig. 3.5. Scanning electron microscopy image of rGO_05/mSiMP electrode **a)** surface morphology **b)** cross-section morphology.

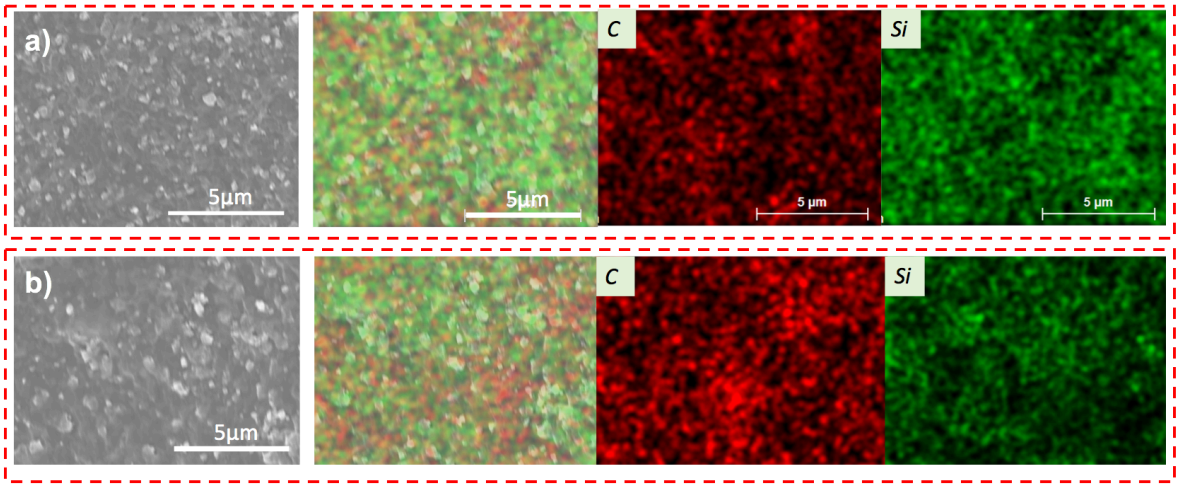

Fig. 3.6. Energy dispersive X-ray image of **a)** rGO_05/mSiMP electrode surface elementary distribution **b)** rGO_40/mSiMP electrode surface elementary distribution.

As shown in **Figure 3.4a**, silicon nanoparticles display an evenly distributed and crack-free rGO_05/SiNP electrode surface, which confirms one of benefits of utilizing air-controlled electrospray in electrode preparation. EDX images (Figure 3.3c and Figure 3.3d) are also strong proofs of previous statement because we can see that both surface and cross-section deliver uniform elementary distributions which can be especially crucial for silicon-based electrode due to silicon's heavy dependence on neighboring conductive agents leads by its intrinsically low electrical conductivity [31]. After further magnified **Figure 3.4a**, we noticed similar micrometer pores found in our group's previous work and these pores can facilitate electrolyte penetration and relax strains during charge/discharge process [14]. Moving to cross-section (Figure 3.7b), a clear layered structure can be observed that SiNPs are wrapped closely by the surrounding rGO flakes and the severe volume expansion/contraction from silicon particles can thus be inhibited by these robust interlayers. These layered structure also delivers a good packing with moderate amount of necessary void spaces and provides us an advanced electrode of relatively high tap density. The smart structure is beneficial from the fact that the size ratio between rGO flakes and SiNPs is relatively large so that rGO can form good coverage and fully

connect SiNPs during charge/discharge process. When lithium ions intercalate on silicon particles, these carbon interlayers are able to prevent electrode degradations by suppressing these severe volume expansions and gathering potentially pulverized active materials together after contraction.

Figure 3.5a and **Figure 3.5b** are rGO_05/mSiMP surface and cross-section SEM images respectively. Even though milled silicon micro-particles have much larger size than that of SiNP, the distribution is not affected by the largely increasing size. Yet instead of layered structure composed of conductive agents and active materials, rGO_05 flakes are not able to fully cover SiMPs and they tend to entangle in between each other (Figure 3.5b). In other words, this kind of structure results in high possibility that silicon particles will not be connected by conductive agents due to lack of aligned rGO flakes. **Figure 3.6a** confirms that when size ratio between rGO and Si is not large enough, electrode surface will not form a good coverage and Si are exposed to outside directly. When we change to larger size rGO, which is S40 in this study, coverage is improved as according to **Figure 3.6a**, silicon exposes less than that in **Figure 3.6b**.

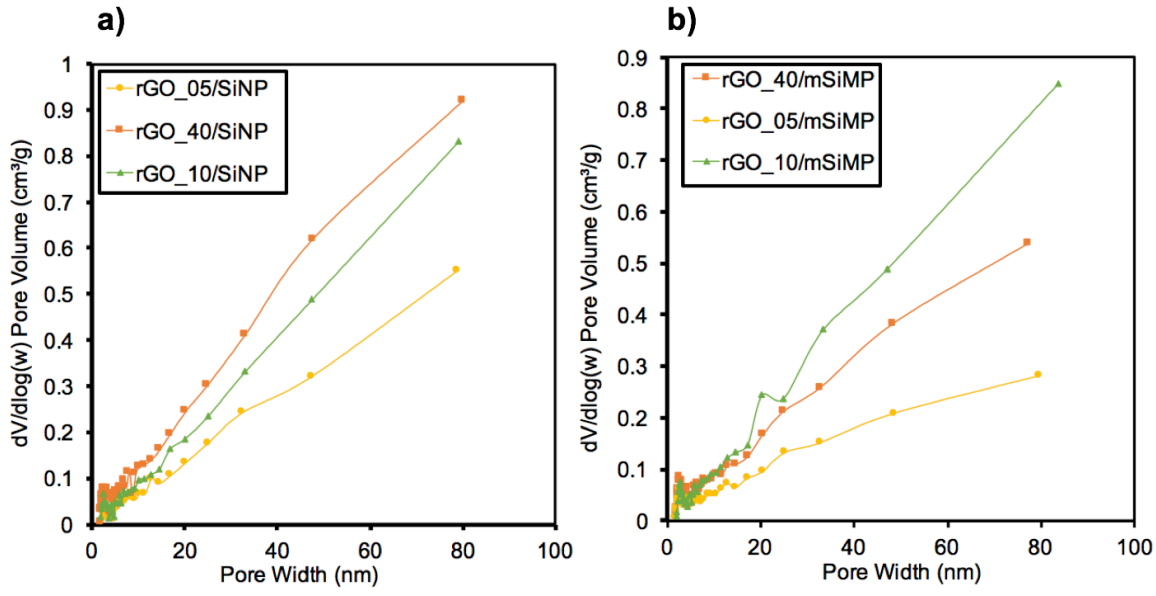

Fig. 3.7. BJH adsorption profiles of **a)** GO/SiNP systems **b)** GO/SiMP systems.

BJH adsorption profiles (Figure 3.7) from BET tests prove that no matter rGO/SiNP or rGO/mSiMP hybrid systems have porous structural natures with great amount of mesopores and larger size pores. From this, we know that those porous structures, favored by electrodes, can be created through air-controlled electrospray, instead of being found coincidently.

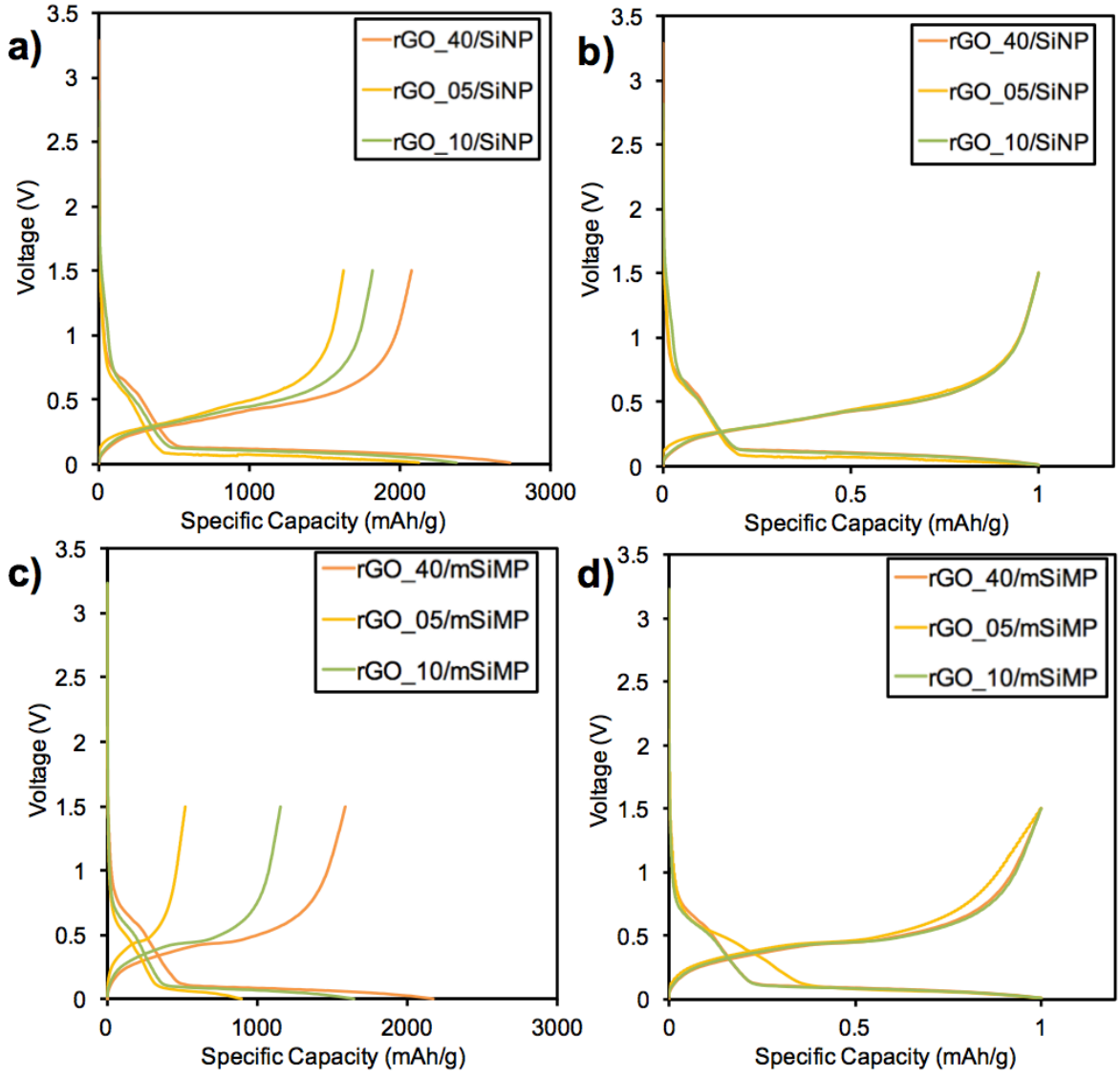

Figure 3.8. capacity-voltage profiles of **a)** rGO_05/SiNP, rGO_10/SiNP and rGO_40/SiNP systems **b)** normalized (based on maximum specific capacity) profile of a) **c)**

rGO_05/mSiMP, rGO_10/mSiMP and rGO_40/mSiMP **d)** normalized (based on maximum specific capacity) profile of c).

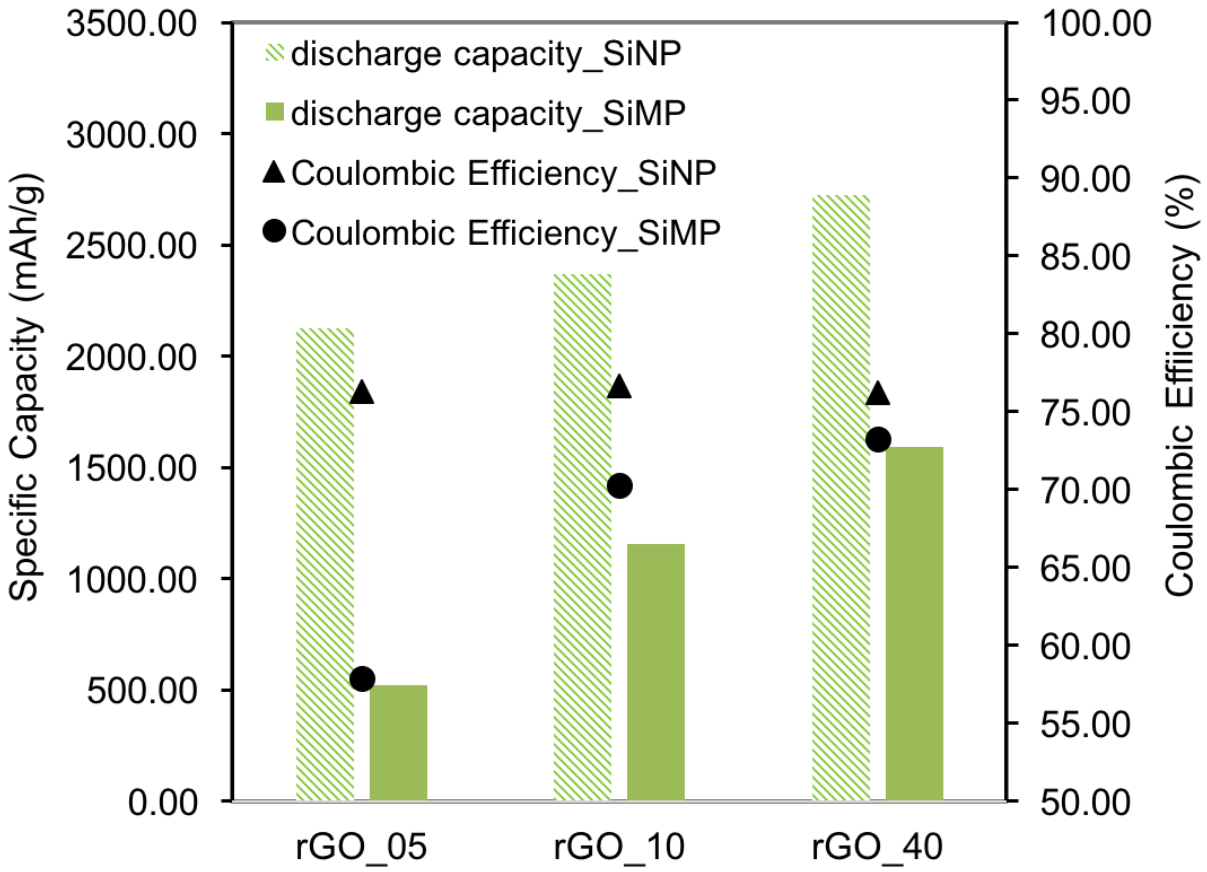

Figure 3.9. 1st cycle discharge capacity and Coulombic efficiency of rGO/SiNP and rGO/mSiMP systems.

Capacity-voltage profiles for these 6 cases are plotted in **Figure 3.8a** and **Figure 3.8c** accordingly. There's a trend that capacities tend to increase with size of GO that involved into the composite systems and the increasing trend is more evident when drawn in histogram (Figure 3.9). This trend matches our previous statement that conductive agents are crucial for silicon-based electrodes. As size of conductive agents get larger, more less-conductive silicon particles are electrically connected and thus utilized. Moreover, this size effect might be more dominant in cases that have mSiMPs as active materials due to the capacity difference between

rGO_05/SiNP and rGO_40/SiNP is around 600 mAh/g whereas difference between rGO_05/mSiMP and rGO_40/mSiMP is much larger, which is over 1000 mAh/g. As silicon particles' size becomes larger, requirement in adequate number of conductive agents also increases in order to maintain active materials to be electrically connected and efficiently utilized. For rGO_05/mSiMP, which includes smallest rGO flakes, its first cycle discharge capacity is less than one fourth of that of rGO_05/SiNP for inefficient silicon utilization (Figure 3.9). Even though improved by increasing conductive agents size, rGO/mSiMP cases in general give lower specific capacity due to insufficient inner conductive pathways.

By checking normalized capacity-voltage profiles (capacities are normalized by maximum capacity), we have better understandings of active materials/conductive agents size ratio effect on electrodes' surface morphologies. For rGO_05/SiNP, rGO_10/SiNP and rGO_40/SiNP, normalized profiles (Figure 3.8b) almost overlap on each other with perfectly matching plateaus positions. These consistencies are evidences of similar chemical reactions happened on electrodes and further illustrate similar electrode surface morphologies. However, as demonstrate before, rGO_05/mSiMP and rGO_40/mSiMP give fairly different surface coverage of active materials (Figure 3.6). Furthermore, profiles for rGO/mSiMP do not overlap on each other (Figure 3.8d). These situations may be explained by difficulty in forming good coverage when active materials sizes are about the same with that of rGO. In other words, we use fishnet [14] as analogy of rGO in this study and mSiMPs will be too big to catch if fishnets have close sizes with those of fishes. Therefore, silicon particles are largely exposed to electrolyte and more SEI will be formed. Since similar extent of coverage, rGO_05/SiNP, rGO_10/SiNP and rGO-40/SiNP show Coulombic efficiency about the same and rGO_05/mSiMP, rGO_10/mSiMP and rGO_40/mSiMP show improved Coulombic efficiency when the "fishnets" getting larger (Figure 3.9).

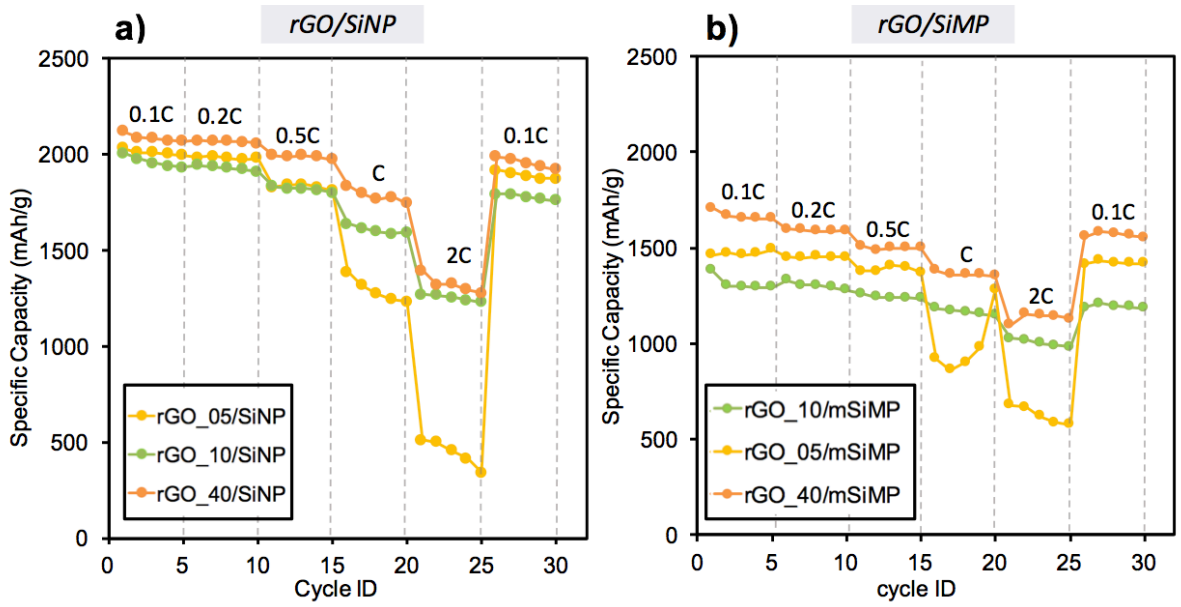

Fig. 3.10. Rate capability test for cells fabricated **a)** rGO/SiNP: rGO_05/SiNP, rGO_10/SiNP and rGO_40/SiNP **b)** RGO/SiMP: rGO_05/mSiMP, rGO_10/mSiMP and RGO_40/mSiMP.

To further distinguish the rGO size effects on systems taken use of SiNPs and mSiMPs as active materials, rate capability tests are conducted on these 6 cases we discussed previously. **Figure 3.10a** depicts performances of rGO/SiNP hybrid systems. Minimum current rate 0.1C means system takes 10 hours to discharge/charge and maximum 2C means system takes 30 minutes to discharge/charge, both are ideal time length when cell is under full lithiation/de-lithiation. When current rate is relatively low, systems show very similar capacities due to adequate conductive pathways, which also matches capacity similarities given at first cycle (Figure 3.9). Differences become more conspicuous when systems moving to the fast-discharge/charge stage (at C and 2C), which raises requirements in efficient conductive pathways that are able to facilitate charge ions movements in shorter time range. Maximum capacity difference can reach to over 1000 mAh g^{-1} between rGO_05/SiNP and rGO_40/SiNP which retain 25% and 65.6% of their initial capacities separately. For rGO_40/SiNP, it still gives 1392.5 mAh g^{-1} specific capacity under C-rate of 2C, which is around four times of that

of traditional graphite anodes at full lithiation and this advantage not only endorses priority of the well-engineered layer-by-layer anodes but also interprets the fact that larger graphene oxide tends to form better-structured conductive networks, which needs further optimization.

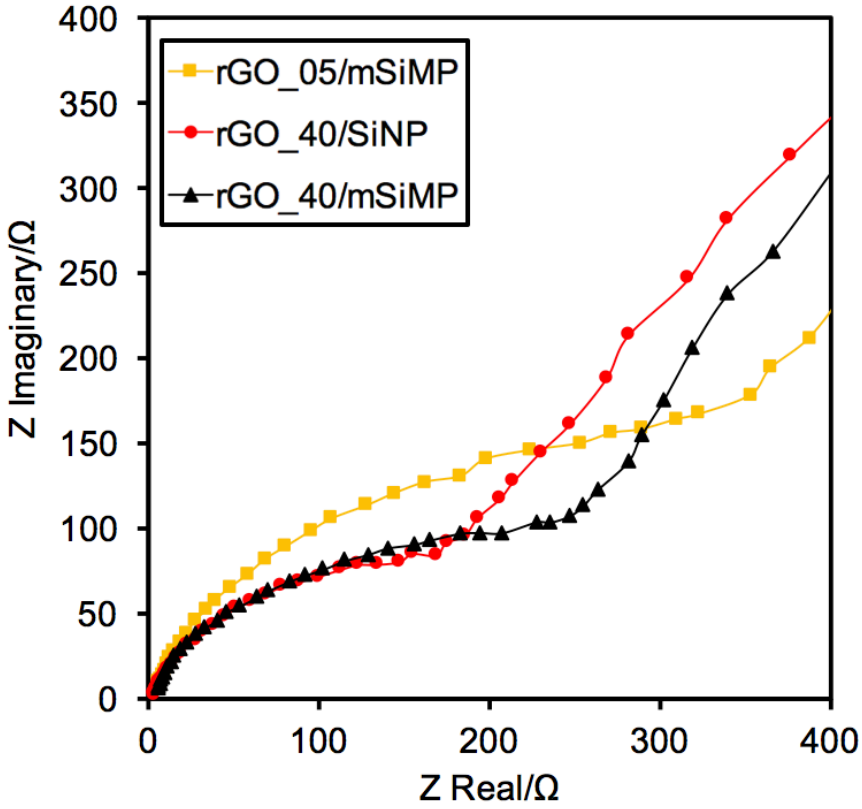

Fig. 3.11. Electrochemical impedance spectroscopy profiles of S40/SiNP, S40/SiMP and Lot.01/SiMP.

Rate capability tests for rGO/mSiMP systems are illustrated in **Figure 3.10b** following the same current rate as in previous tests. In general, capacities are lower than rGO/SiNP cases which is consistent with results shown in **Figure 3.9**. EIS result (Figure 3.11) helps to explain the occurrence of capacity difference. Electrodes have smaller inner charge transfer impedance when there's a well-built conductive network so that Li ions go through shorter solid-state diffusion length and electrical connection of SiNPs will be easier comparing with mSiMPs

when same size of rGO is chosen. Even though capacities cannot reach as high as rGO/SiNP systems, there's no drastic capacity loss, which is actually common to happen in electrodes with SiMP involved [32] and rate capabilities are even improved. 67.6%, 74.2% and 46.4% of their original specific capacities are retained at current rate of 2C for rGO_05/mSiMP, rGO_10/mSiMP and rGO_S40/mSiMP accordingly, which are higher than those in rGO/SiNP systems. There might be several reasons to explain this improvement: first, insufficient silicon utilization palliates potential system degradation caused by severe volume expansion and contraction so that structural integrity can be better maintained and conductive pathways function well; second, these ball milled silicon micro-particles might be able to form a more compact electrode structure due to its disk shape and removal of extra functional groups expedite lithium ions movement which even though leads to lower specific capacity, improves electrode's ability to support fast charging/discharging.

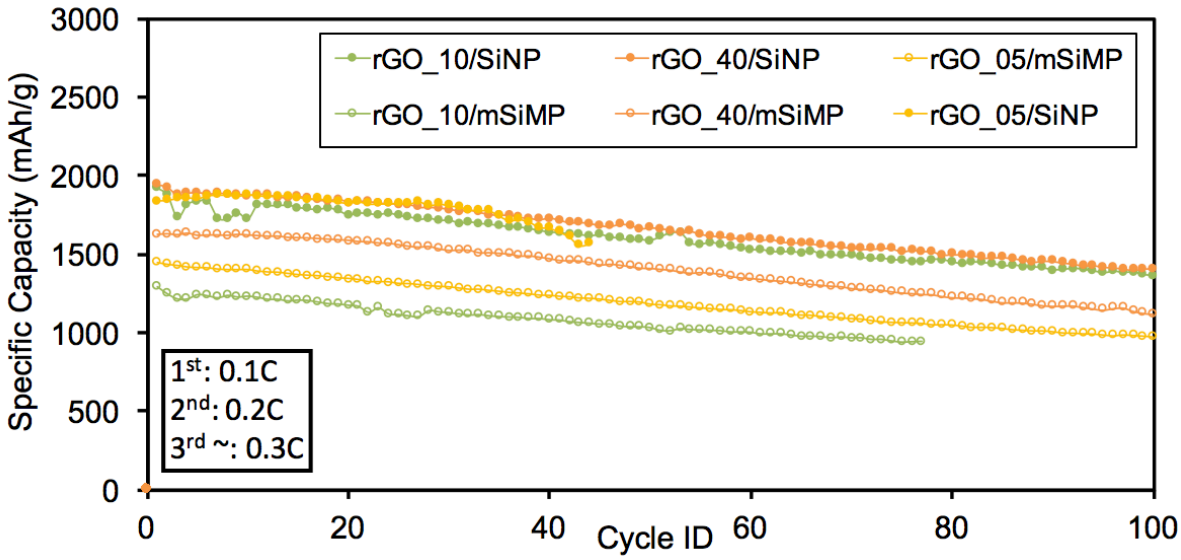

Fig. 3.12. Cyclic performance of rGO/SiNP (rGO_05/SiNP, rGO_10/SiNP and rGO_40/SiNP) and rGO/mSiMP (rGO_05/mSiMP, rGO_10/mSiMP and rGO_40/mSiMP) under current rate of 0.3C.

Again, we observe similar trends by looking into individual cases that electrodes use largest rGO as conductive agents has the best rate-capability test which is under expectations. However, specific capacities all have prominent improvements comparing those in first cycle and this increase may due to silicon micro-particles' pulverization during cycling, which is more affected to happen than silicon nanoparticles [33]. As silicon particles start to degrade into smaller size, we can imagine that more fresh active materials will expose to electrolyte and due to existence of conductive agents, broken bulk silicon particles are in use. Cycling profiles (Figure 3.12) can illustrate systems' abilities to hold structural integrity during long-term discharge/charge processes, which is another essential measurement of whether electrode has capability of being commercialized. According to the results, we see two information: first, these 6 cases deliver very similar trends in cycling. These similar trends illustrate the fact that rGO layered structure may be able to gather active materials firmly and is compatible with different sizes and shapes. However, as we mentioned previously, systems have large silicon particles involved commonly show fast capacity decay. Possible reason to explain this improvement is that current conductive agents in rGO/mSiMP are not be enough for full utilizations of silicon micro-particles, which is also confirmed by capacities differences in between rGO/SiNP and rGO/mSiMP. There's a trade-off in between higher initial capacity/Coulombic efficiency and stable cycle retention with fair capacity that gradually increases during cycling. Second information is even though specific capacities are relatively close in three rGO/SiNP cases, differences in those of rGO/mSiMP can be clearly observed. This result has consistencies with previous rate-capability results and confirms the fact that when larger active materials are taken into use, system raises up requirements on adequate conductive pathways in order to reach efficient utilizations.

3.4 Conclusion

In this work, directly deposited GO/Si hybrid systems are prepared via air-controlled electrospray method. Systems then go through thermal annealing under mild conditions in order to reduce graphene oxides and achieve more electrically conductive rGO/Si electrodes. rGO assembled networks function as conductive agents which can facilitate Li ions movements by shortening their solid-state diffusion pathways and assist more efficient silicon utilization. Possible size ratio effects on systems' morphology and packing conditions from various graphene oxide and silicon particles are further explored in this study by choosing three graphene oxide in addition with two silicon particles varied in size. It is found that specific capacity has an increasing trend with increasing graphene oxide trends in both rGO/SiNP and rGO/mSiMP hybrid systems due to better formed electrode conductive networks in systems when larger GO are involved. When larger active materials are chosen, requirements in adequate conductive agents is more important as capacity difference in between rGO_05/mSiMP and rGO_40/mSiMP is much evident comparing with that of rGO_05/SiNP and rGO_40/SiNP. Moreover, rGO/mSiMP have lower specific capacities in general comparing with rGO/SiNP, which is because the fact that silicon micro-particles are more difficult to be utilized under same conductive networks built inside of systems. Furthermore, difference in coulombic efficiency indicates various extent of surface coverage. rGO/SiNP cases in general are better covered than rGO/mSiMP due to the fact that GO flakes are much larger than SiNP. As rGO reduce direct contact between active materials and electrolyte, less SEI is formed during initial stage, which leads to high coulombic efficiency. Since size ratios between each kind of rGO and SiNP are big and form similar surface morphologies, coulombic efficiencies among rGO/SiNP are very close. On contrary, rGO/mSiMP cases have an obvious increasing trend with increasing rGO size because of better and better surface coverage. Even though electrochemical performances are not ideal initially for rGO/mSiMP, self-improvements in specific capacities are noticed during cycling because of mSiMP gradual

pulverization, which creates smaller silicon particles and are well connected by conductive agents. These systems are capable of maintaining stable cycling and have even better rate-capability tests results than rGO/SiNP. This inspires us a lot, especially in industrial perspective, silicon micro-particles are less functionalized since their larger size boosts difficulty level in building conductive networks that can create electrical connect between active materials. However, if appropriate size of conductive agents can be chosen, in our study, rGO_40, system can thus give fair specific capacity and comparable cycle retention with rGO_40/SiNP. Moreover, due to less silicon is utilized, potential in structural degradation also decreases and system will not show huge capacity decay even under current rate of 2C. In this study, all rGO/mSiMP cases have specific capacities over 1000 mAh g^{-1}, which is much higher than theoretical capacity of traditional graphite anode. If further consider cost effect, mSiMPs have nearly two order of magnitude smaller production cost than that of SiNPs. Even though we cannot achieve capacities as high as the condition that mSiMP is substituted with SiNP, we are still able to fulfill requirements from fast-growing electric vehicle market on higher capacity and fast-charging with much cheaper milled silicon micro-particles.

References

[1] M. Armand, J.M. Tarascon, Building better batteries. Nature. 451 (2008) 652-657. doi:10.1038/451652a.

[2] L. Ji, Z. Lin, M. Alcoutlabi, X. Zhang, Recent developments in nanostructured anode materials for rechargeable lithium-ion batteries. Energy & Environmental Science. 4 (2011) 2682-2699. doi:10.1039/c0ee00699h.

[3] N. Kim, C. Oh, J. Kim, J.S. Kim, E.D. Jeong, J.S. Bae, T.E. Hong, J.K. Lee, High-performance Li-ion battery anodes based on silicon-graphene self-assemblies. Journal of The Electrochemical Society. 164 (2017) A6075-A6083. doi: 10.1149/2.0101701jes.

[4] Y. Sun, G. Zheng, Z. Seh, N. Liu, S. Wang, J. Sun, H.R. Lee, Y. Cui, Graphite-encapsulated Li-metal hybrid anodes for high-capacity Li batteries. Chem. 1 (2016) 287-297. doi:10.1016/j.chempr.2016.07.009.

[5] U. Kasavajjula, C. Wang, A.J. Appleby, Nano- and bulk-silicon-based insertion anodes for lithium-ion secondary cells. Journal of Power Sources. 163 (2007) 1003-1039. doi:10.1016/j.jpowsour.2006.09.084.

[6] C.K. Chan, R.N. Patel, M.J. O'Connell, B.A. Korgel, Y. Cui, Solution-grown silicon nanowires for lithium-ion battery anodes. ACS Nano. 4 (2010) 1443-1450. doi:10.1021/nn901409q.

[7] C.K. Chan, H. Peng, G. Liu, K. Mcllwrath, X.F. Zhang, R.A. Huggins, Y. Cui, High-performance lithium battery anodes using silicon nanowires. Nat Nanotechnol. 3 (2008) 31-35. doi: 10.1038/nnano.2007.411.

[8] M.H. Park, M.G. Kim, J. Joo, K. Kim, J. Kim, S. Ahn, Y. Cui, J. Cho, Silicon nanotube battery anodes. Nano Lett. 9 (2009) 3844-3847. doi:10.1021/nl902058c.

[9] X. Liu, J. Zhang, W. Si, L. Xi, B. Eichler, C. Yan, O.G. Schmidt, Sandwich nanoarchitecture of Si/reduced graphene oxide bilayer nanomembranes for Li-ion batteries with long cycle life. ACS Nano. 9 (2015) 1198-1205. doi:10.1021/nn5048052.

[10] M. Fang, Z. Wang, X. Chen, S. Guan, S. Sponge-like reduced graphene oxide/silicon/carbon nanotube composites for lithium ion batteries. Applied Surface Science. 436 (2018) 345-353. doi:10.1016/j.apsusc.2017.11.070.

[11] L. Xiao, Y. H. Sehlleier, S. Dobrowolny, H. Orthner, F. Mahlendorf, A. Heinzel, C. Schulz, H. Wiggers, Si–CNT/rGO nanoheterostructures as high-performance lithium-ion-battery anodes. ChemElectroChem. 2 (2015) 1983-1990. doi:10.1002/celc.201500323.

[12] Y. Chen, Y. Hu, Z. Shen, R. Chen, X. He, X. Zhang, Y. Zhang, K. Wu, Sandwich structure of graphene-protected silicon/carbon nanofibers for lithium-ion battery anodes. Electrochimica Acta. 210 (2016) 53-60. doi:10.1016/j.electacta.2016.05.086.

[13] L. Fei, S.H. Yoo, R.A.R. Villamayor, B.P. Williams, S.Y. Gong, S. Park, K. Shin, Y.L. Joo, Graphene Oxide Involved Air-Controlled Electrospray for Uniform, Fast, Instantly Dry, and Binder-Free Electrode Fabrication, ACS Appl. Mater. Interfaces. 9 (2017) 9738–9746. doi:10.1021/acsami.7b00087.

[14] K.S. Novoselov, A.K. Geim, S.V. Morozov, D. Jiang, Y. Zhang, S.V. Dubonos, I.V. Grigorieva, A.A. Firsov, Electric Field Effect in Atomically Thin Carbon Films. Science. 306 (2004) 666-669. doi:10.1126/science.1102896.

[15] R. Raccichini, A. Varzi, S. Passerini, B. Scrosati, The role of graphene for electrochemical energy storage. Nature Materials. 14 (2015) 271-279. doi:10.1038/NMAT4170.

[16] X. Tong, H. Wang, G. Wang, L. Wan, Z. Ren, J.T. Bai, J.B. Bai, Controllable synthesis of graphene sheets with different numbers of layers and effect of the number of graphene layers on the specific capacity of anode material in lithium-ion batteries. Journal of Solid State Chemistry. 184 (2011) 982-989. doi:10.1016/j.jssc.2011.03.004.

[17] E. Yoo, J. Kim, E. Hosono, H. Zhou, T. Kudo, I. Honma, Large reversible Li storage of graphene nanosheet families for use in rechargeable lithium ion batteries. Nano Letters. 8 (2008) 2277-2282. doi:10.1021/nl800957b.

[18] R. Mukherjee, A.V. Thomas, A. Krishnamurthy, N. Koratkar, Photothermally reduced graphene as high-power anodes for lithium-ion batteries. ACS Nano. 6 (2012) 7867-7878. doi:10.1021/nn303145j.

[19] H. Wang, L.F. Cui, Y. Yang, H.S. Casalongue, J.T. Robinson, Y. Liang, Y. Cui, H. Dai, Mn3O4−graphene hybrid as a high-capacity anode material for lithium ion batteries. J. Am. Chem. Soc. 132 (2010) 13978–13980. doi:10.1021/ja105296a.

[20] C. Fu, G. Zhao, H. Zhang, S. Li, Evaluation and Characterization of Reduced Graphene Oxide Nanosheets as Anode Materials for Lithium-Ion Batteries. Int. J. Electrochem. Sci. 8 (2013) 6269-6280.

[21] S. Park, R.S. Ruoff, Erratum: Chemical methods for the production of graphenes. Nature Nanotechnology. 5 (2010) 309-309. doi:10.1038/nnano.2010.69.

[22] K.S. Kim, Y. Zhao, H. Jang, S.Y. Lee, J.M. Kim, K.S. Kim, J.H. Ahn, P. Kim, J.Y. Choi, B.H. Hong, Large-scale pattern growth of graphene films for stretchable transparent. Nature. 457 (2009) 706-710. doi:10.1038/nature07719.

[23] A. Reina, X. Jia, J. Ho, D. Nezich, H. Son, V. Bulovic, M.S. Dresselhaus, J. Kong, Large area, few-layer graphene films on arbitrary substrates by chemical vapor deposition. Nano Letters. 9 (2009) 30-35. doi:10.1021/nl801827v.

[24] F. Li, X. Jiang, J. Zhao, S. Zhang, Graphene oxide: A promising nanomaterial for energy and environmental applications. Nano Energy. 16 (2015) 488-515. doi:10.1016/j.nanoen.2015.07.014.

[25] N. Zaaba, K. Foo, U. Hashim, S. Tan, W. Liu, C. Voon, Synthesis of graphene oxide using modified Hummers Method: Solvent influence. Procedia Engineering,184 (2017) 469-477. doi:10.1016/j.proeng.2017.04.118.

[26] D. Chen, H. Feng, J. Li, Graphene oxide: Preparation, functionalization, and electrochemical applications, Chem. Rev. 112 (2012) 6027–6053. doi:10.1021/cr300115g.

[27] J. Chang, X. Huang, G. Zhou, S. Cui, P.B. Hallac, J. Jiang, P.T. Hurley, J. Chen, Lithium-ion batteries: Multilayered Si nanoparticle/reduced graphene oxide hybrid as a high-performance lithium-ion battery anode. Advanced Materials. 26 (2014) 665-665. doi:10.1002/adma.201470028.

[28] D. Pan, S. Wang, B. Zhao, M. Wu, H. Zhang, Y. Wang, Z. Jiao, Li storage properties of disordered graphene nanosheets. Chemistry of Materials. 21 (2009) 3136-3142. doi:10.1021/cm900395k.

[29] C. Wang, D. Li, C.O. Too, G.G Wallace, Electrochemical Properties of Graphene Paper Electrodes Used in Lithium Batteries. Chemistry of Materials. 21 (2009) 2604-2606. doi:10.1021/cm900764n.

[30] N. Liu, Z. Lu, L. Zhao, M.T. Mcdowell, H. Lee, W. Zhao, Y. Cui, A pomegranate-inspired nanoscale design for large-volume-change lithium battery anodes. Nature Nanotechnology. 9 (2014) 187-192. doi:10.1038/NNANO.2014.6.

[31] W. Liu, Z. Guo, W. Young, D. Shieh, H. Wu, M. Yang, N. Wu, Effect of electrode structure on performance of Si anode in Li-ion batteries: Si particle size and conductive additive. Journal of Power Sources.140 (2005) 139-144. doi:10.1016/j.jpowsour.2004.07.032.

[32] S. Choi, T. Kwon, A. Coskun, J.W. Choi, J. W. Highly elastic binders integrating polyrotaxanes for silicon microparticle anodes in lithium ion batteries. Science. 357 (2017) 279-283. doi:10.1126/science.aal4373.

Chapter 4

Future Work: Interconductivity from Graphene Nanoribbon (GNR) in Directly Deposited Silicon/Graphene Li-ion Batteries Anode

4.1 Motivations

This future work is inspired by one of our group's previous works [1], which developed LIB anodes composed of poly(vinyl alcohol)(PAA)/silicon/graphene nanoribbon(GNR) composite fibers via water-based electrospinning method. By taking use of GNR's superior conductivity, this kind of advanced LIB anode showed huge enhancement in specific capacity and capability, especially at high rate. In this previous study, GNR functioned as electrode inner conductive pathways which were capable of overcoming potential contact loss in between active materials accompanied with Li^+ insertion and removal [2]. Contact loss is a huge issue for silicon nanoparticle based electrode because of the drastic volume expansion/contraction happens during cycling aggravates active materials alteration and pulverization [3]. Moreover, due to GNR's inherent structural stability and strong mechanical strength [4], we believe that adding GNR as additives will also be beneficial in maintaining system's long-term cycle retention.

However, there's an intrinsic drawback hinders this idea into industrial application. Since electrode is prepared through directly deposition of fiber onto cupper collector, system structure turned to be relatively loose due to void spaces in between fibers [1]. These void spaces could accommodate strain relaxing during cycling, however, further reduce electrode tap density meanwhile. Low tap density is one issues owned by silicon nanoparticles and many researchers have attempted to develop SiNP/C composite LIB anode to address this issues [5]. We already known air-controlled electrospray method is able to produce GO/SiNP LIB anode effectively with good layer-structured packing from Chapter 3. Based on these studies, we might want to investigate how GNR affect electrode system of higher packing density as

additives. In order to achieve this goal, different amount of GNR (1wt%, 2wt%, 5wt%) can thus be added into pre-made slurry with other actively materials and directly deposited onto copper collector via air-controlled electrospray method. Adjustments were made in solution preparation comparing with that of GO/SiNP out of purpose to simplify experimental process. First, we substituted GO with graphene so that thermal annealing step can be skipped and furthermore, we added around 20wt% polyacrylic acid (PAA) for better active material attachment.

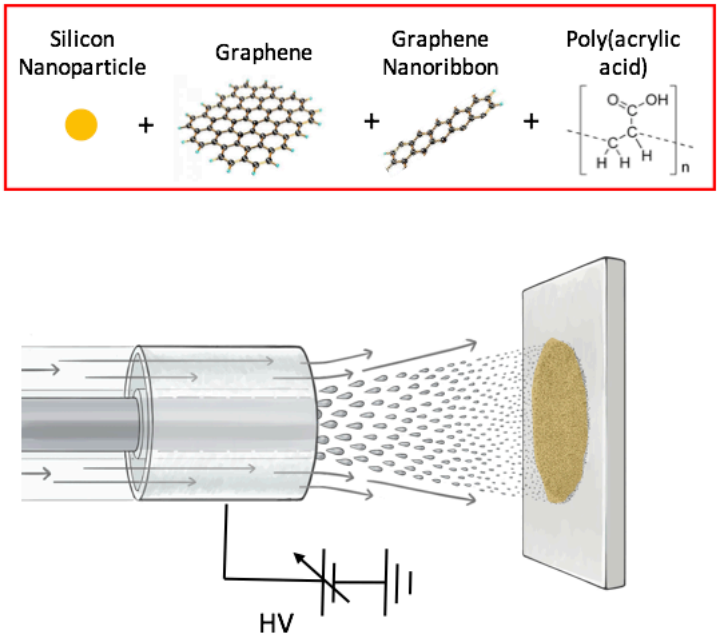

Fig. 4.1. Schematic illustrations of air-controlled electrospray process for Si/Graphene/GNR nanostructured electrode preparation.

4.2 Experimental Details

0.5g 5wt% PAA (MW 3 MDa, Sigma-Aldrich) solution, which was half of total binder solution, was first mixed with 4.0 g DI water and 0.2g SiNP (US Research Nanomaterials Inc., 98+%, 30-50 nm) was added until the PAA-water mixture was stirred to homogenous phase. The

solution then went through half-hour sonication (Qsonic) and 5-hour stirring for better dispersion. Total amount of carbon materials (graphene/GNR) was kept to be same in solution and reference case (0wt% GNR) contained 1.4g Graphene solution (ACS Materials, 6wt% graphene sheets). For other cases, different amount of graphene solution was substituted by GNR according to the ratio we set. Solution was sonicated again and stirred for several hours before spray and the last step was adding the other half of binder solution. We intentionally did "half-half" method so that PAA's binding ability could be well retained. Electrospray conditions were 20cm working distance, 25kV voltage, 30psi air pressure and 0.03mL/min infusion rate, as shown in **Figure 4.1**. Moreover, Disks were stored in vacuum oven at 100ºC overnight before cell assembly to avoid ambient moisture that could affect electrochemical performances.

Half cells (2032-CR) were assembly in an argon-filled glovebox. Prepared SiNP/Graphene/GNR or SiNP/Graphene discs were used as anodes and lithium foil was selected as counter electrode, which were separated by Polypropylene membrane (Celgard). Electrolyte was $LiPF_6$ (1M) in ethylene carbonate and dimethyl carbonate (50:50 wt/wt%) with 10 wt% fluoroethylene carbonate as additive. Galvanostatic charge/ discharge process was tested on battery analyzer (MTI) under 0.01 – 1.5V voltage window versus Li/Li^+ with 2 initial formation cycles at 0.18 Ag^{-1} for cell activation. Cycling tests were then performed at both 1.26 A g^{-1} and 4.2 A g^{-1} (0.3C and C). Capacities reported were calculated into specific capacities, which count total weight of disc excluding copper substrates. In following discussion, No GNR represented system did not contain any GNR, 1% GNR meant system contained 1wt% GNR as additives and 2% GNR and 5wt% GNR correspondingly.

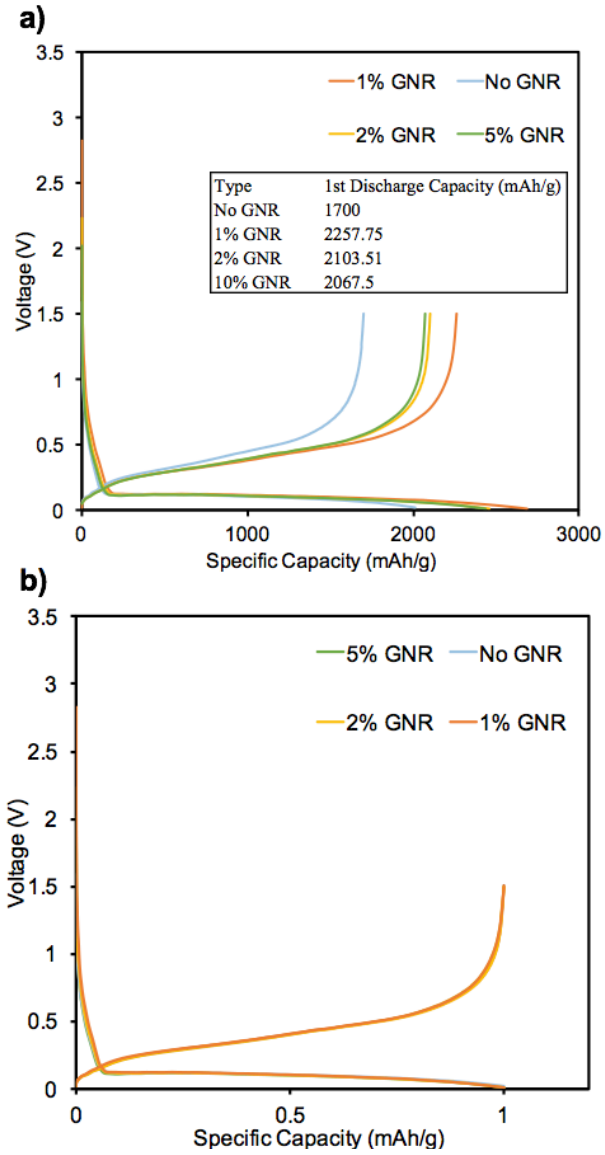

Figure 4.2. a) capacity-voltage profiles of Gr/SiNP composite electrodes with 0wt%, 1wt%, 2wt% and 5wt% GNR as additives and corresponding 1st cycle specific discharge capacity. **b)** plot a)'s normalized version (for SEI comparison).

4.3 Results and Discussions

Since silicon contents are controlled to be same, only difference between samples is the number of conductive agents (GNR) incorporated into system. The initial capacity-voltage profile (Figure 4.2a) of these 4 cases shows that for the case does not involve GNR has lower specific capacity comparing with those contain GNR in general, which confirms that GNR is able to

increase contact between active materials and facilitate Li^+ movement by increasing electrode inner conductive pathways. However, increases in specific capacities are not correlated with increase in GNR content and disc adding only 1wt% GNR exhibited highest capacity at formation cycle, which are shown in the plot. **Figure 4.2b** is normalized version of **Figure 4.2a**, specific capacities are normalized into range from 0 to 1 according to the largest capacity and resulting profiles almost overlap on each other. Similar profile shape illustrated that solid-electrolyte-interface (SEI) formations happen around same for these cases, which should be ascribed to the truth that instead of surface morphology, GNR additives affect mostly on electrode inner geometry.

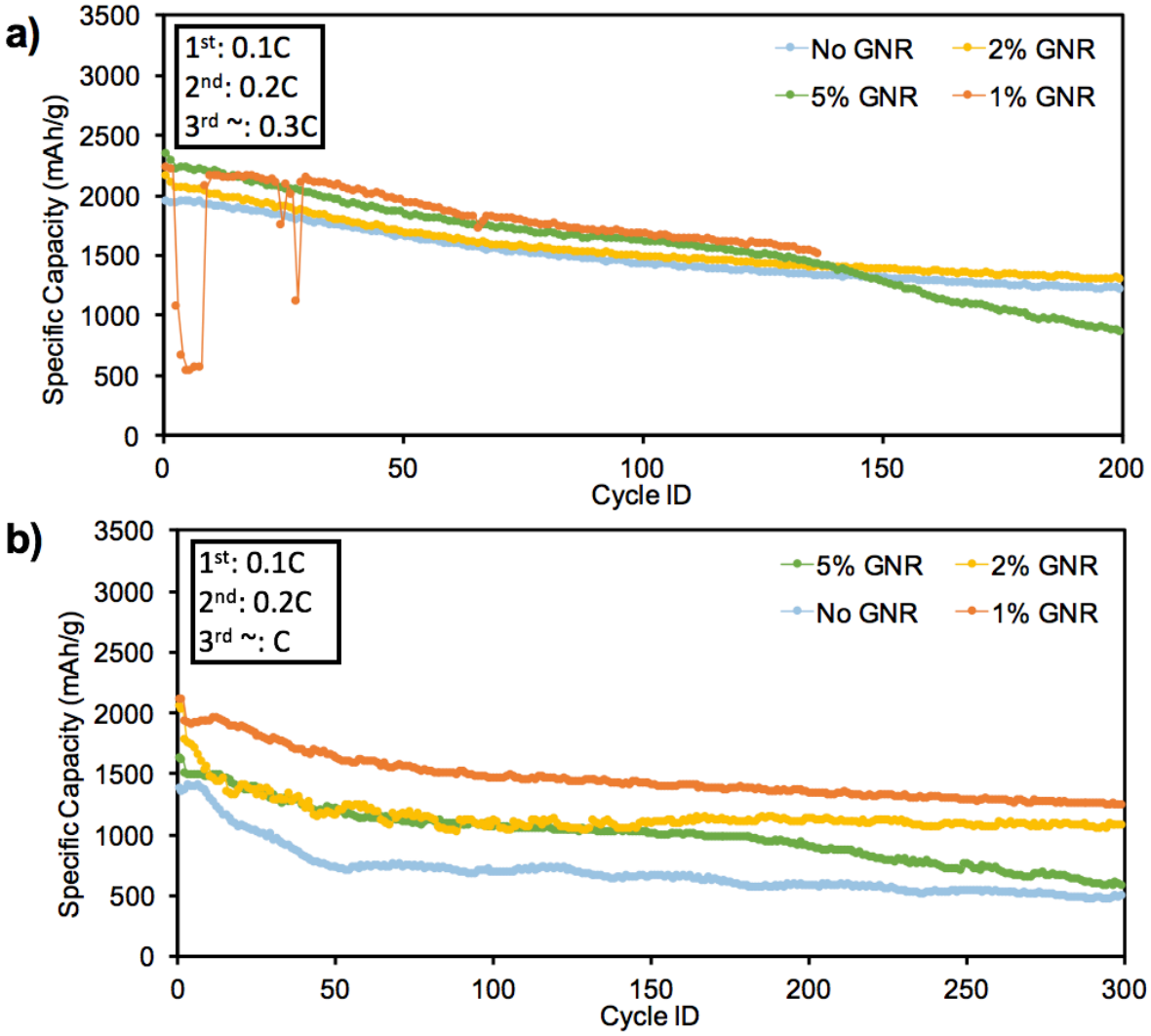

Figure 4.3. galvanostatic discharge/charge profiles of Gr/SiNP composite electrodes with 0wt%, 1wt%, 2wt% and 5wt% GNR as additives at current rate **a)** 0.3C and **b)** C.

Figure 4.3a and **Figure 4.3b** show cyclic performances of discs with different GNR contents at current rate 1.26 A g^{-1} (0.3C) and 4.2 A g^{-1} (C) accordingly. At relatively slow current, capacities do not differ drastically and cycling profiles are almost parallel during first 100 cycles (except 1% GNR shows some unstable outliers). Slight differences in capacity may be explained by the fact that Li ions were capable of moving properly in between electrodes at relatively low current rate, however, notable difference were observed at high current rate (Figure 4.3b). In order for battery to charge/discharge at fast rate, existence of adequate number of conductive pathways to facilitate Li ion movements may be more essential than that at low current rate. Systems with GNR as additives all show much higher specific capacities comparing with reference case (No GNR), especially at first 100 cycles. At 100^{th} cycle, specific capacities are retained at 685.35 mAh g^{-1}. 1478.42mAh g^{-1}, 1034.82 mAh g^{-1} and 1052 mAh g^{-1} for No GNR, 1% GNR, 2% GNR and 5% GNR accordingly. Largest capacity difference could reach almost 800 mAh g^{-1} and confirms GNR's superior property as electrode conductive agent.

	No GNR	1% GNR	2% GNR	5% GNR
% Retention (100 cycles)	49.21	77.66	59.58	70.70
% Retention (300 cycles)	34.85	64.64	62.04	38.71
% Reduction (per cycle)	0.22	0.12	0.13	0.20
Specific Capacity (mAh/g) (after 300cycles)	485.36	1230.56	1077.55	576.00

Table 4.1. Cycle retention for No GNR, 1wt% GNR, 2wt% GNR and 5wt% GNR at current rate of C.

Moreover, GNR brings not only increase in specific capacity, but also more stable system integrity maintenance when the amount added is chosen appropriately. GNR involved systems retained 10% to 20% more capacities than No GNR case during first 100 cycles and exhibit less capacity reduction per cycle during first 300 cycles, which are shown in **Table 4.1**. However, we notice specific capacity decay after 100 cycles for 5wt% GNR case at both current rates, there's no definite reason to explain why this situation happened. Normally, severe capacity decay is accompanied with electrode degradation during the charging/discharging process. Moreover, 2 wt% GNR and 5 wt% GNR's cyclic profiles almost overlap before first 100 cycles, which might mean that GNR has limited effects on increasing system's inner conductivity and system might reach to "saturated state" if excess GNR is added. "Saturated" in this study refers to the situation that when system contains too much GNR, instead of assisting Li ions mobilizing, excessive GNR starts to cause damage to system because of its potential high volumetric density. Our guess is that optimization of GNR is between 1wt% to 2wt%, which requires further work to prove. Even though this work is at initial phase, it has already enlightened us the key position that conductive agent stands for silicon-based electrodes. Furthermore, optimization in GNR composition is important because of the potential damage it could cause to the system integrity. Details will be elaborated in Future Work section.

4.4 Future Works

In order to optimize GNR usage, series of characterizations could be very helpful. Physical characterizations such as transmission electron microscopy (TEM) and cross-section images from scanning electron microscopy (SEM) will illustrate how GNR interact and involve in electrode structure and if we can find GNR clusters as increasing GNR composition, it can be used as valid proof that excess GNR does cause damage to system structure and won't function

properly comparing with sparsely ordered GNR. Electrochemical characterization such as electrochemical impedance spectroscopy (EIS) is also a straightforward measurement of system's inner conductivity. If EIS can be conducted for each case, we could plot a trend between electrode inner resistance and amount of GNR. Rate capability can be performed if we want to further explore how system behave at even higher current rate. Even though has not been completed due to time constrains, this work so far still shows promising result that adding moderate conductive agents helps maintaining silicon-based LIB anode high specific capacity (1230.56 mAh g-1) after 300 cycles at relatively fast current rate. Hopefully this work could be finished soon in our group with these fundamental works.

References

[1] G. Shoorideh, B. Ko, A. Berry, M.J. Divvela, Y.S. Kim, Z. Li, P. Patel, S. Chakrapani, Y.L. Joo, Harvesting Interconductivity and Intraconductivity of Graphene Nanoribbons for a Directly Deposited, High-Rate Silicon-Based Anode for Li-Ion Batteries. ACS Applied Energy Materials. 1 (2018) 1106-1115. doi:10.1021/acsaem.7b00228.

[2] J. Yang, M. Winter, J.O. Besenhard, Small particle size multiphase Li-alloy anodes for lithium-ionbatteries. Solid State Ionics. 90 (1996) 281-287. doi:10.1016/s0167-2738(96)00389-x.

[3] N. Liu, Z. Lu, L. Zhao, M.T. Mcdowell, H. Lee, W. Zhao, Y. Cui, A pomegranate-inspired nanoscale design for large-volume-change lithium battery anodes. Nature Nanotechnology. 9 (2014) 187-192. doi:10.1038/NNANO.2014.6.

[4] R. Faccio, P.A. Denis, H. Pardo, C. Goyenola, A.W. Mombrun, Mechanical properties of graphene nanoribbons. J. Phys.: Condens. Matter. 21 (2009) 285-304. doi:10.1088/0953-8984/21/28/285304.

[5] D. Lin, Z. Lu, P. Hsu, H.R. Lee, N. Liu, J. Zhao, H. Wang, C. Liu, Y. Cui, A high tap density secondary silicon particle anode fabricated by scalable mechanical pressing for lithium-ion batteries. Energy & Environmental Science. 8 (2015), 2371-2376. doi:10.1039/c5ee01363a.